Published in final edited form as:
Mol Pharm. 2009 ; 6(5): 1290–1306. doi:10.1021/mp900018v.

Magnetic Nanoparticle Drug Carriers and their Study by Quadrupole Magnetic Field-Flow Fractionation

P. Stephen Williams*, **Francesca Carpino**, and **Maciej Zborowski**
Department of Biomedical Engineering, Lerner Research Institute, Cleveland Clinic, 9500 Euclid Avenue, Cleveland, OH 44195, USA.

Abstract

Magnetic nanoparticle drug carriers continue to attract considerable interest for drug targeting in the treatment of cancers and other pathological conditions. The efficient delivery of therapeutic levels of drug to a target site while limiting nonspecific, systemic toxicity requires optimization of the drug delivery materials, the applied magnetic field, and the treatment protocol. The history and current state of magnetic drug targeting is reviewed. While initial studies involved micron-sized and larger carriers, and work with these microcarriers continues, it is the sub-micron carriers or nanocarriers that are of increasing interest. An aspect of magnetic drug targeting using nanoparticle carriers that has not been considered is then addressed. This aspect involves the variation in the magnetic properties of the nanocarriers. Quadrupole magnetic field-flow fractionation (QMgFFF) is a relatively new technique for characterizing magnetic nanoparticles. It is unique in its capability of determining the distribution in magnetic properties of a nanoparticle sample in suspension. The development and current state of this technique is also reviewed. Magnetic nanoparticle drug carriers have been found by QMgFFF analysis to be highly polydisperse in their magnetic properties, and the strength of response of the particles to magnetic field gradients is predicted to vary by orders of magnitude. It is expected that the least magnetic fraction of a formulation will contribute the most to systemic toxicity, and the depletion of this fraction will result in a more effective drug carrying material. A material that has a reduced systemic toxicity will allow higher doses of cytotoxic drugs to be delivered to the tumor with reduced side effects. Preliminary experiments involving a novel method of refining a magnetic nanoparticle drug carrier to achieve this result are described. QMgFFF is used to characterize the refined and unrefined material.

Keywords

Magnetic nanoparticles; Magnetic drug targeting; Drug carriers; Magnetic field-flow fractionation; Magnetic refinement

Introduction

Non-specificity of chemo- and radio-therapies is a major hindrance to the effective treatment of well defined tumors. When cytotoxic drugs or radiotherapeutic agents are administered to the blood stream, they are systemically distributed, and healthy cells are attacked in addition to the tumor cells. This limits the dose that can be safely administered to the patient and reduces the potential effectiveness of the drug or radiotherapeutic agent for the tumor cells. Targeting of the cytotoxic agent to the tumor cells offers the potential for allowing the administration of higher localized drug doses while reducing the dose to non targeted areas. The focusing of

*Corresponding author. Telephone: 1-216-444-1217. Fax: 1-216-444-9180. willias3@ccf.org.

magnetic drug-carrying particles using localized magnetic fields remains a potentially effective approach to the targeting of cytotoxic agents.

Magnetic Microcarriers for Drug Targeting

The transport of fine magnetic particles carrying radioactive materials or drugs through the vascular system with their subsequent focusing at localized parts of the body using magnetic fields was proposed by Freeman, Arrott, and Watson in 1960.[1] Meyers and co-workers[2, 3] were shortly afterwards able to demonstrate the magnetic focusing of intra-arterially injected 1 to 3 μm radioactive iron (^{59}Fe) particles in dogs. In 1971, Nakamura et al.[4] reported the localized capture of magnetic particles introduced into the blood circulation of both rats and dogs. Magnetic drug targeting was first explored in the late 1970s and through the 1980s; this early literature being reviewed in 1989 by Gupta and Hung.[5] Micron-sized and larger magnetic carriers, such as erythrocytes,[6–9] liposomes,[10, 11] emulsions,[12–15] starch microspheres,[16, 17] and albumin microspheres,[18–38] were generally used over this period, although in 1984 Ishii et al.[39] described some *in vitro* studies using submicron magnetic liposome drug carriers. The carriers were in each case loaded with magnetic nanoparticles and a chemo- or radio-therapeutic agent. The magnetic fields used to target the carriers were provided by simple magnets or magnetic pole pieces placed over the targeted area. The strength of the field was considered to be sufficient if the induced magnetophoretic velocity of a microsphere carrier particle exceeded the estimated mean blood flow velocity in the arterio-capillary blood supply to the tumor.[40] Ovadia et al.[41] pointed out that typical magnetic carriers are essentially saturated at 4000 Gauss (0.4 T) and that the magnitude of the field gradient then governs their focusing. This was consistent with their observation of the focusing of magnetic carriers at the edges of their magnet pole piece where the field gradients were highest, a phenomenon they referred to as the "edging effect." Targeting an area with the face of a simple magnet could result in focusing of magnetic drug carriers more strongly to cells adjacent to the target. They proposed that the edge effect could be used to target specific areas by careful orientation and positioning of the magnet.

Interest in the use of these relatively large microcarriers (i.e., magnetic carriers larger than 1 μm in diameter) has continued to the present day. They are considered by some to be advantageous because magnetic forces due to interaction with magnetic field gradients are expected to be large enough to counter hydrodynamic forces due to blood flow in the larger blood vessels. They could be captured from blood flow by applying an external magnetic field.[42–55] The capture of magnetic microparticles from blood flow could also be enhanced by implanting magnetizable needles, wires, beads,[56–61] or stents.[62–64] It has even been suggested that magnetically labeled stem cells could be targeted to specific parts of the body using external magnetic fields.[65] The modeling of magnetic microcarrier capture can be carried out by trajectory calculations (see, for example, refs. [19, 47, 50–52, 54, 56–60, 62, 63, 66]), since Brownian diffusion is negligible. In the special cases of implanted needles, wires, or stents that are magnetized by an external magnetic field, the theory initially developed for high gradient magnetic separation (HGMS)[67–71] could be adapted.[56–58, 60, 62, 63] There are certain drawbacks associated with the use of magnetic microcarriers, however. For example, they may be large enough to cause blockage of smaller capillaries, and have a greater tendency to aggregate which may exacerbate the problem.[72] Also, their circulation time tends to be shorter than that of smaller particles, as they tend to be taken up by the reticuloendothelial system (RES) more quickly, as discussed below.

Magnetic Nanocarriers for Drug Targeting

Goodwin et al.[73, 74] observed extravasation of magnetic carriers (iron/carbon particles of diameter 0.5 to 5 μm, with 95% < 3 μm) in targeted areas of the liver in pigs. This, they claimed,

was a mechanism for retention of the carriers at the targeted site after the removal of the magnetic field. The same magnetic carriers incorporating doxorubicin were later used for a study of intravesical magnetic targeting of the bladder wall in healthy pigs using an externally applied neodymium-iron-boron (NdFeB) magnet (0.5 T).[75] Following a 30 minute exposure to the magnet the carriers were found to be retained within the layers of the epithelium at the targeted sites. Smaller magnetic carriers tend to extravasate more easily than microcarriers, and extravasation into tumors is aided by the higher microvascular permeability and higher interstitial diffusion observed for both carrier and drug in neoplastic tissue.[76–78] A study of a human colon adenocarcinoma in immunodeficient mice indicated a vascular pore cut-off of between 400 and 600 nm.[79] A later study of a variety of tumor types has shown that most exhibit a vascular pore cutoff size between 380 and 780 nm.[80] In addition, it has also been observed that intracellular uptake of particles increases as size is reduced, and nanoparticles are preferentially taken up in comparison to microparticles.[81–83] This is important because uptake of the carrier particles into the tumor cells can be a contributing mechanism for the efficient delivery of the drug. Studies[84–87] of liposomes circulating in the blood system (see also refs. [88, 89]) had revealed that circulation times were a function of their size as well as the chemistry, surface charge, and rigidity of their surface membrane. Smaller, unilamellar liposomes (< ~200 nm diameter) were not so quickly taken up by the reticuloendothelial system (RES) as larger multilamellar liposomes. A sufficiently long circulation time is also important for maximizing the possibility of capture at the targeted site. The various factors involved in the extension of circulation time and transfer of drug to the cell have been reviewed.[90–92]

In 1997, Lübbe and co-workers carried out the first Phase I clinical trial of magnetically targeted nanoparticles to deliver the anti-cancer drug 4'-epidoxorubicin to advanced solid tumors in 14 patients[93, 94] (see also the discussion following publication[95, 96]). The carriers were approximately 50 to 150 nm in diameter, and consisted of clusters of ferrofluid particles (magnetite), coated with anhydroglucose polymer, on the surface of which the drug was reversibly adsorbed. The magnetic fields were provided by NdFeB magnets arranged on the skin close to the tumor. Magnetic fields of at least 0.5 T and up to 0.8 T were measured on the poles of the magnets, and these could be placed within 0.5 cm of the tumor surface. There was no estimate given of the field gradients in the region of the tumors. Results of treatment were considered positive for half of the patients included in the study. They suggested that further optimization was required, including the consideration of using larger microcarriers of up to 1 μm in diameter that would respond more strongly to the magnetic field. They later published fuller discussions of the factors relevant to successful drug targeting in their experimental studies.[97, 98] Lübbe and co-workers[99, 100] later carried out an extensive study on VX-2 squamous cell carcinoma tumors in a rabbit model. They used the same ~100 nm magnetic carriers with a suitable anticancer drug, and focused the particles using a 1.7 T electromagnet with a specially designed pole shoe that enhanced the field gradient at its tip. It was estimated that the field fell to 1.0 T and the field gradient was 30 T/m at a distance of 1 cm below the pole tip. An effective dose of the drug alone resulted in complete remission of the tumors but with severe side effects. On the other hand, with magnetic targeting, the drug dose could be reduced by a factor of 2 to 5 and still bring about complete remission with relatively mild side effects.

Liposome drug carriers of mean diameter 146 nm or 86 nm, containing only one or two 10 nm magnetite particles each, were targeted in the case of a hamster osteosarcoma model with either an implanted permanent magnet (cylindrical, 5 mm diameter, 5 mm length),[101, 102] or an externally applied magnetic field (0.3 to 0.4 T).[103] The combination of the implanted magnet and 146 nm liposome carriers gave rise to a 4-fold increase in delivery of anticancer drug to the tumor compared to intravenous free drug infusion, and the external magnetic field with 86 nm liposomes gave a 3- to 4-fold increase.

As mentioned above, research in magnetic drug targeting has shifted in favor of nano-sized magnetic carriers in recent years; see, for example, refs. [61, 104–148]. This area of research has also been the subject of several comprehensive reviews.[91, 149–156] Capture experiments have been reported *in vitro* 113, [117, 127, 157] and *in vivo*,[122, 127, 146] but generally with only estimates given of field and field gradient. Magnetic fields used for focusing of magnetic nanocarriers have been modeled and measured in three-dimensional space,[99, 109, 147] and theoretical models involving trajectory calculations have been developed.[53, 61, 131, 134] Theoretical treatments and modeling have not taken into account the effects of Brownian diffusion of the nanocarriers, even though there have been several theoretical treatments of HGMS of magnetic nanoparticles published.[158–162] The one exception is a theoretical treatment by Cotten and Eldredge[163] that dealt with the modeling of capture of magnetic nanoparticles. They built upon an earlier model proposed by Ebner, Ritter, and Ploehn[164] that concerned heteroflocculation of particles of different size and different composition in a magnetic field. In each case the value of the Peclet number (*Pe*), which is a measure of the ratio of magnetic and Brownian forces, was taken to determine when capture occurs. Cotten and Eldredge took the conservative threshold of $Pe > 10$ to define capture. In addition, the polydispersity in the magnetic properties of the nanocarriers has not been considered, partly because, until recently, there was no way of measuring the magnetic polydispersity. (Polydispersity in overall size of the nanocarriers was generally noted.) The consideration of the polydispersity in the magnetic properties of the drug carrier is critically important for the development of effective magnetic targeting because the presence of a significant fraction of weakly magnetic drug carriers in a formulation will contribute to systemic toxicity. The depletion of the weakly magnetic fraction from a polydisperse formulation will therefore reduce systemic toxicity, and allow the use of higher and more effective drug dosage.

In this work we report preliminary experiments involving the depletion of the less magnetic fraction of a magnetic drug carrier formulation using a magnetic flow-through device. The magnetic properties of the refined and unrefined formulations were determined using quadrupole magnetic field-flow fractionation.

Field-Flow Fractionation

The two closely related separation techniques, field-flow fractionation (FFF)[165–168] and split-flow thin channel (SPLITT) fractionation,[169–172] were invented by J. Calvin Giddings at the University of Utah. The initial concept for each of the systems was based on separation within a fluid that is driven along a thin, planar, parallel-walled channel with a field applied across the thin dimension of the channel, perpendicular to the flow. The majority of systems still utilize channels of planar geometry. The materials separated range from polymeric materials in solution, through colloids, up to particles of tens of microns in diameter.

Field-flow fractionation (FFF) is an analytical technique that is similar in some ways to chromatography. As in chromatography, a separation of a small sample into its components is achieved within a flow of a carrier fluid along a separation channel. Whereas chromatography exploits differences in partition between mobile and stationary phases to separate sample components as they are carried along a column, FFF separation is achieved within the flowing mobile phase alone and does not utilize a stationary phase. The FFF channel need not be planar, but it must be thin, and have a cross section of high aspect ratio and a constant thickness. A field or field gradient of some type must be applied across the channel thickness. The nanoparticles to be separated interact with the field or field gradient and are driven toward one of the channel walls. The increase of particle concentration close to the wall is opposed by diffusion and a steady-state concentration distribution is quickly approached in the thin channel. In the ideal case, it is assumed that there is no particle-particle or particle-wall

interaction. For a uniform collection of nanoparticles, the steady state concentration profile then takes the form

$$c(x)=c_0 \exp\left(-\frac{x|u|}{D}\right)=c_0 \exp\left(-\frac{x}{w\lambda}\right) \quad (1)$$

where $c(x)$ is the local concentration at distance x from the channel wall, c_0 is the concentration at the channel wall, $|u|$ is the magnitude of the particle velocity toward the wall due to its interaction with the field, D is the particle diffusion coefficient, w is the channel thickness, and the dimensionless λ is the so-called retention parameter. This is given by

$$\lambda=\frac{D}{|u|w}=\frac{kT}{|F|w} \quad (2)$$

in which k is the Boltzmann constant, T is the absolute temperature, and $|F|$ is the magnitude of the force on a single particle toward the wall due to its interaction with the field. The final form on the right hand side of eq (2) is obtained by substituting the Stokes-Einstein equation for D ($D = kT / f$, where f is the particle friction coefficient), and realizing that $u = F / f$. The influence of particle friction coefficient on the diffusion coefficient and on the field-induced velocity cancels, and the concentration profile is seen to be a function of only the force experienced by the particles. Particles that interact strongly with the field form thin steady-state zones close to the wall, while particles that interact less strongly form more diffuse steady-state zones. With the flow of fluid along the channel, having a parabolic velocity profile with maximum velocity at the channel center and zero velocity at the walls, those particles that are confined to thin zones next to the wall are carried more slowly than those forming more diffuse zones. The elution times for the particles are therefore a function of the strength of their interaction with the applied field; those that interact weakly elute before those that interact more strongly. A chromatographic detector at the channel outlet yields an elution curve of particle concentration as a function of elution time that is known as a fractogram.

For a plane, parallel-plate channel, the elution time t_r for a steady-state zone of uniform particles is given by

$$t_r=\frac{t^0}{R}=\frac{t^0}{6\lambda(\coth(1/2\lambda)-2\lambda} \approx \frac{t^0}{6\lambda(1-2\lambda)} \approx \frac{t^0}{6\lambda} \quad (3)$$

in which t^0 is the time for a non retained material to pass through the channel, and R is the so-called retention ratio. The penultimate form on the right hand side is accurate to within 0.37% for $\lambda < 0.15$, while the final approximation is the limiting form for $\lambda \rightarrow 0$ (in fact, it is only 10% in error at $\lambda = 0.05$).

As mentioned earlier, most implementations of both FFF and SPLITT fractionation have employed plane, parallel-plate geometry. The first FFF channels were constructed using two flat-faced blocks, clamped around a thin spacer (usually Teflon, Mylar, or polyimide) out of which the channel outline had been cut. Ducts through the blocks conveyed the carrier solution to and from the ends of the channel. Planar channels are suited to those fields that can be applied uniformly across the thickness of the channel. Such channels are still in use for gravitational,[173–175] thermal,[176–178] electrical,[179, 180] and flow[181, 182] FFF. The design was modified for sedimentation FFF where the channel is wrapped around a centrifuge basket.[183] However, the centrifugal field in this case still acts uniformly across the channel thickness. There has been

some success in development of hollow fiber flow FFF which uses a permeable capillary tube as the channel.[184–186] In this case the out-flow through the tube walls exerts a radial drag force on the particles. Quadrupole magnetic FFF (QMgFFF) uses a quadrupole magnetic field in which field increases linearly from the axis in all directions. Such a field is axisymmetric, implying no dependence on angular direction. A channel occupying an annular space within the aperture of the quadrupole field is therefore optimum.

Magnetic Field-Flow Fractionation

Prior to the development of quadrupole magnetic FFF there were several attempts to develop magnetic FFF but, for various reasons, they did not result in much success. Vickrey and Garcia-Ramirez,[187] Mori,[188] and, more recently, Williams and co-workers[189] used tubular channels with transverse field gradients. Such an arrangement is far from ideal.[167, 190] Mori[188] demonstrated only slight retardation of Ni^{2+} complexes with BSA, egg albumin, and EDTA. Williams et al.[189] were able to show some retention of 12.5 nm $CoFe_2O_4$ particles relative to the suspending fluid.

Schunk, Gorse, and Burke[191, 192] used a parallel-plate channel with a magnetic field provided by an electromagnet. A maximum field of about 275 Gauss (0.0275 T) and field gradient of about 21 Gauss/mm (2.1 T/m) were obtainable, with less than 1% variation in field along the length of the channel. They were able to separate singlet from doublet 0.8 μm rod-shaped iron oxide particles used in the recording industry (i.e., fairly large, high susceptibility particles). The relatively weak field and field gradient would be insufficient to retain particles that are much smaller than those separated.

In 1986, Semenov and Kuznetzov[193] suggested a very different approach to the design of a magnetic FFF system. They proposed that a ferromagnetic wire be placed at the axis of a tubular channel mounted perpendicular to a uniform magnetic field. The field magnetizes both the wire and the particles to be separated. They presented calculations that suggested that retention of both paramagnetic and diamagnetic particles would be possible in such a system. The coaxial channel geometry is also not ideal for FFF, however. The force on retained particles would rapidly increase as the wire is approached, which would tend to induce particle capture. Also, the force is not axisymmetric around the wire, but alternates between attraction and repulsion at 90-degree intervals. Therefore, only a fraction of the small surface of the wire would serve as the accumulation wall, which would make the system highly susceptible to overloading. In the same year, Semenov[194] proposed a parallel plate magnetic FFF channel in which the field would be provided by the induced magnetization of parallel ferromagnetic wires arrayed uniformly in the surface of one of the walls. The wires were to lie in the direction of flow, and the field was to be applied across the channel thickness. He presented a theoretical study of the proposed system and concluded that it would be more efficient than the coaxial system. Such an arrangement would help to alleviate overloading, although the strong spatial variation in force on the particles would remain. It will be appreciated that the use of ferromagnetic wires in a magnetic field results in very short range high gradient magnetic fields, on the order of the wire diameter, that are more suited to particle capture as in the high gradient magnetic separation (HGMS) systems.[67, 159, 161]

From 1994, Ohara and co-workers[195–203] have pursued an approach to magnetic FFF similar in concept to that proposed by Semenov.[194] The majority[195–202] of their publications describe theoretical studies and simulations. They refer to the technique as magnetic chromatography, even though no partition between phases is involved. In 2002, Mitsuhashi et al.[203] reported an experimental implementation with which they were able to show slight retention of some transition metal salts, although band spreading was extremely high.

A theoretical study of a system referred to as magnetic FFF was presented in 2001.[204] However, although the system involved a flow of fluid in a parallel plate channel with a transverse magnetic field, the model did not describe FFF in its accepted sense.

Quadrupole Magnetic Field-Flow Fractionation

Quadrupole magnetic field-flow fractionation (QMgFFF)[205–209] makes use of a quadrupole magnetic field that has the property of being axisymmetric. Inside the aperture of the quadrupole, the magnitude of the magnetic field increases in direct proportion to the distance from the axis. The gradient in magnetic field is therefore constant within the aperture and is directed away from the axis. A thin helical channel is used to exploit the axisymmetric field. The channel is machined into the surface of a precision-turned, hard polymer rod (Delrin™ from du Pont) that fits tightly into an internally polished stainless steel tube.[206–208] The channel is mounted in the aperture of the quadrupole magnet such that the tube makes close contact with the pole pieces. The channel is thereby held axisymmetrically with the field. The magnitude of the magnetic field is therefore constant and maximized at the outer channel wall, and the field gradient across the channel thickness is constant throughout the channel. If is assumed that there is no interaction between particles, as for other forms of FFF, then the dependence of R on λ for the helical channel would deviate only to a small extent from that shown in eq (3) which is valid for the parallel-plate channels.[209] The dependence converges to the relationship in eq (3) as $w / r_o \rightarrow 0$.

QMgFFF separates magnetic nanoparticles according to their response to the magnetic field gradient. It is precisely this property that is exploited for magnetic targeting, and the range of variation of the response is of critical importance when highly cytotoxic drugs are to be confined to specific areas of the body. The force $\mathbf{F}_m$ (vector quantities are depicted in bold face) on a magnetized particle in a magnetic field gradient is given by the equation

$$\mathbf{F}_m = V_m M \nabla B \tag{4}$$

in which V_m is the volume of magnetized material incorporated in the particle, M is the magnetization of this material in the magnetic field, and ∇B is the gradient in the magnetic field (a vector). The other components making up the nanoparticle, including coatings and cytotoxic drugs, will generally have insignificant response to the magnetic field. In a quadrupole field, the gradient of the magnetic field is directed away from the axis and, as mentioned above, is constant and equal to B_o / r_o where B_o is the magnitude of the field at the outer wall of radius r_o. In the quadrupole field, the magnitude of force F_m on a magnetized particle is directed away from the axis, and is given by

$$F_m = V_m M B_o / r_o \tag{5}$$

Consideration of eqs (2), (3), and (5) shows that, with knowledge of the dependence of M on B, the fractogram may be transformed into a volume or mass distribution curve of magnetite (or any other magnetic material) among the particles.[208] The polydispersity of the particulate material with respect to magnetic material content is therefore obtained. The transformation requires only knowledge of the magnetization curve (magnetization M as a function of magnetic field B) for the magnetic material incorporated into the particles. More importantly, the volume or mass distribution of magnetic material is directly related to the distribution in the strength of the response of the magnetic drug carriers to a non uniform magnetic field. It is important to point out that QMgFFF yields the distribution in the strength of interaction with a magnetic field without any assumption regarding the shape of that distribution, such as a normal or log-normal distribution. This property is of critical relevance to the effectiveness of

magnetic targeting where it is the least magnetic fraction that is expected to contribute most to systemic toxicity.

Volume distributions of magnetite V_m in the particles may be transformed into distributions of equivalent spherical diameters d_m of magnetite. It may be seen from eqs (2), (3), and (5) that, under a given set of experimental conditions, the elution time for particles increases in almost direct proportion to the volume of magnetite V_m, and therefore, with the cube of the equivalent spherical diameter of magnetite d_m. In the terminology of separation science, the separation is considered highly selective with respect to d_m. The selectivity with respect to d_m is defined by the equation

$$S(d_m)=\frac{d\ln t_r}{d\ln d_m}=\frac{d_m}{t_r}\frac{d\,t_r}{d\,d_m} \tag{6}$$

and we see that $S(d_m)$ approaches 3. This high selectivity presents a problem for the analysis of polydisperse materials under constant conditions. Particles having a 3-fold difference in d_m would have a 27-fold difference in elution time. It is not only the inconvenience of widely differing elution times that is the problem; the more strongly retained fractions become increasingly diluted in the outlet stream. The dilution of the more strongly retained fractions reduces their detectability. A technique to circumvent this problem is to gradually reduce the field gradient during the elution of a sample. This is known as field decay programming, or simply field programming. It is analogous to solvent programming in liquid chromatography or temperature programming in gas chromatography.

The procedure for analysis of a polydisperse nanoparticulate sample is briefly described as follows. A small sample of a suspension of the nanoparticles is introduced to the sample loop of an injection valve. The current to the electromagnet is set to some initial level, and the sample is carried onto the channel using a relatively slow flow rate of carrier fluid. The carrier fluid flow is then interrupted, and the sample particles are allowed to reach their steady state distribution across the channel thickness under stopped flow conditions. The carrier fluid flow is then re-established at some flow rate selected for the elution. At the same time, the programmed decay of current to the electromagnet, which produces the desired decay in field gradient, is initiated. This may consist of some initial period where the field gradient is held constant, followed by a decay of field gradient that follows some mathematical function of time. This results in a timely elution of the more magnetic fractions of a sample, while adequately retaining the lesser magnetic fractions at the initial high field gradient. The nanoparticles are eluted in the order of increasing strength of interaction with the magnetic field gradient.

Adaptation of QMgFFF to Refinement of Magnetic Drug Carrier Formulations

The very high selectivity of QMgFFF may be exploited to carry out small, batch-wise binary, or indeed higher order, fractionations of polydisperse magnetic particulate materials. Such fractionations may be accomplished by employing step functions in magnetic field gradient. A single step yields a binary fractionation, two steps a ternary fractionation, and so on. The concept may be explained as follows for a simple binary fractionation. Suppose the sample is introduced to the channel at some initial magnetic field gradient that is sufficient to retain a fraction of the particle population at a retention ratio of less than 0.1 (corresponding to $\lambda <$ 0.0173), for example. The majority of this fraction will be retained to a much stronger degree, of course. However, those particles carrying less magnetite will be retained to a much lesser degree. If the channel is then flushed with around 10 channel volumes of carrier fluid, the retained fraction will remain in the channel. In fact, the more strongly retained material in this

fraction will remain close to the channel inlet. The particles carrying less magnetite will be carried off the channel by the flow of carrier fluid, and these may be collected if desired. The removal of the channel from the magnetic field gradient then allows the retained particles to redistribute across the channel thickness (a process known as secondary relaxation in the FFF terminology) and be carried from the channel by the continuing flow of fluid and be collected in a second fraction. The step-wise reduction in field gradient may be carried out under stopped flow conditions or without interruption of flow.

This relatively crude methodology constitutes a significant advance in selection for the more magnetic fraction of a nanoparticle drug formulation. The approach to steady state distribution across the channel thickness is relatively fast because of the small thickness of the channel. The magnetic field and field gradient is uniform throughout the channel. The volume of sample that may be loaded on the channel can be relatively large. For analytical purposes, where separation efficiency is important, sample volumes are usually small compared to channel volume. However, a simple binary fractionation does not require high efficiency. The sample particles carrying larger amounts of magnetite will start to relax to the wall during sample loading, and this is facilitated by loading at slow carrier flow rates. If the object of the fractionation is to collect only the more magnetic fraction, then it is possible to load a sample having a volume comparable to the channel volume, or even exceeding the channel volume. There will tend to be a build up of magnetic particle concentration in the channel, particularly close to the channel inlet, but this should not adversely affect the fractionation. Some of the less magnetic particles may be carried out of the channel during the period of sample loading, but if the interest is in collecting only the more magnetic fraction then this is unimportant.

Experimental Section

Materials

The magnetic nanoparticle drug carrier was kindly provided by the laboratory of Dr. Vinod Labhasetwar (Department of Biomedical Engineering, Lerner Research Institute, Cleveland Clinic). The preparation of the material has been described in the literature.[119, 210, 211] The particles were water-dispersible oleic acid-Pluronic-coated iron oxide magnetic nanoparticles. They may be loaded with hydrophobic anticancer agents that partition into the oleic acid coating around the iron oxide core. The outer coating of Pluronic F-127 on the particles served to stabilize their suspension in water. The particles used in this study did not carry a drug, but the mechanism of fractionation of the magnetic nanoparticles is not influenced by the inclusion or absence of drug.

The preparation of the magnetic nanoparticles involves several steps. Firstly, the iron oxide nanoparticles are prepared. These are coated with oleic acid, and, being unstable in aqueous suspension, form a precipitate. Excess oleic acid is removed by washing with de-ionized water. Plurionic is added to an aqueous dispersion of the particles, and this is stirred overnight in a closed container to avoid oxidation of the magnetic iron oxide. Finally, the magnetic nanoparticles are captured by placing a 12,200 G (1.22 T) magnet on the side of the vessel. This allowed repeated washing with de-ionized water to remove excess Pluronic. The vessel typically contained 45 mL of suspension. The migration distances across the vessel were therefore substantial, and the field and field gradient consequently varied widely across the vessel. This approach to capture of magnetic particles is not unusual, but there would be no discrimination between capture of strongly or weakly magnetic particles.

The mean hydrodynamic diameter of the magnetic nanoparticles was determined by dynamic light scattering to be 193 nm with a distribution corresponding to a relative standard deviation of 0.262. The diameter of the iron oxide core particles was determined by transmission electron microscopy (TEM) to be 11 ± 2 nm.[119]

The de-ionized water at the Lerner Research Institute, Cleveland Clinic is supplied by an in-house reverse osmosis system, maintained by Western Reserve Water Systems, Inc. (Cleveland, OH) and Cleveland Clinic Facilities Engineering. This water is subsequently passed through a Milli-Q water system (Millipore Corp., Billirica, MA). The carrier fluid used for sample dilution and for sample elution from the QMgFFF system was Milli-Q water. The magnetic nanoparticles were very stable in suspension in de-ionized water.

Equipment

The QMgFFF system has been described previously.[206–208] The quadrupole electromagnet was designed and assembled in our laboratory. It consisted of four AWG 18 coated copper wire coils, each of nominally 1900 m length, wound around 1018 low carbon, cold rolled steel plates, 6.00 in (15.24 cm) tall and 1.00 in (2.54 cm) thick. The coils were obtained from Coil Winding Specialist (CWS, Santa Ana, CA). One end of each plate was machined to the necessary hyperbolic profile to generate an axisymmetric field gradient in an aperture of 16 mm diameter. This was carried out by the Cleveland Clinic Prototype Laboratory. The copper wire coils had measured electrical resistances of between 35.6 and 35.8 Ω. The field return paths were facilitated with a square yoke of 1018 low carbon, cold rolled steel. This was also made of 6.00 in (15.24 cm) tall plates, but of 0.75 in (1.91 cm) thickness. A schematic of the cross section of the electromagnet plates and coils has been shown in the literature.[207] A photograph of the quadrupole electromagnet is shown in Figure 1. The stainless steel tube housing the helical FFF channel is shown above the quadrupole aperture. It is lowered into the aperture during experiments for particle analysis. The power for the electromagnet was provided by a Xantrex HPD60-5 regulated DC Power Supply having a nominal maximum current of 5 A at 60 V (Xantrex Technology Inc., British Columbia, Canada). The electromagnet was capable of generating a maximum field of 0.71 T at the pole tips. The power supply was controlled by computer using a GPIB interface (also from Xantrex Technology Inc.). The decay of field during sample analysis could be programmed according to any desired function of time. The field at the position of the outer channel wall was monitored using a Model 6010 Gauss/Tesla Meter (SYPRIS, Test & Measurement, F. W. Bell, Orlando, FL). The field was recorded during the elution of samples at a position adjacent to the channel and a correction applied to obtain the field at the channel wall. The output of the Gauss meter was recorded to a data file using a 12-bit analog-to-digital converter (DI-154RS, Dataq Instruments, Akron, OH) and the company's Windaq Lite software.

The channel was machined to a depth of 250 μm into the surface of a precision-turned Delrin™ (du Pont) rod of 0.586 in (1.488 cm) diameter and 6.20 in (15.49 cm) length. The helical path made four complete revolutions around the rod. It had an overall length of 23.5 cm, and a breadth of about 1.6 cm, giving a nominal volume of 0.94 mL. The inlet and outlet ports were machined into the ends of the rod, and tapped for chromatography fittings. This work was carried out by Criterion Tool & Die, Inc. (Brook Park, OH). The Delrin™ rod was inserted into a tightly fitting, internally-polished stainless steel (316 grade) tube of outer diameter 0.625 in (1.588 cm) and wall thickness 0.020 in (0.051 cm). This was accomplished by cooling the two components in liquid nitrogen, assembling them, and allowing the assembly to return to room temperature.

A Waters 515 HPLC pump (Waters Corp., Milford, MA) was used to drive the carrier fluid. The samples for analysis were introduced to the channel using a 7725i Rheodyne injection valve (Rheodyne, Cotati, CA) with a 20 μL injection loop. The 20 μL loop was replaced with a 100 μL loop for the refinement experiments. A Model VUV-12 HPLC UV-detector (fixed wavelength 254 nm, HyperQuan, Inc., Colorado Springs, CO) was used to detect the eluting particles at the channel outlet. The detector output was recorded to data file using the same 12-bit analog-to-digital converter as used for the Gauss meter.

Characterization of Magnetic Nanoparticles Using Programmed QMgFFF

The magnetic nanoparticle suspension, as supplied by the laboratory of Dr. Labhasetwar, was diluted 1:10 using Milli-Q water (Millipore Corp., Billierica, MA). Iron content before dilution was 2.58 mg/mL. The water was degassed and filtered using a 0.22 μm pore Millipore filter prior to use for sample dilution and as carrier fluid. An initial field of 0.592 T at the outer channel wall was applied. Before introducing a sample to the QMgFFF channel, it was sonicated to disrupt any aggregates that may have formed. The suspension was remarkably stable, and no sedimentation was ever observed. A 20 μL sample of the diluted suspension was introduced to the channel using the injection valve and a loading flow rate of 0.10 mL/min for 2 minutes. This period was required to carry the sample through the connecting tubing and onto the channel. The flow was stopped for 30 minutes to allow the sample particles to relax to their steady state distributions across the channel thickness. The carrier flow was then reestablished at 0.5 mL/min, and the field gradient decay program initiated at the same time. The current to the electromagnet was controlled to obtain a field gradient decay according to the power program function:[212]

$$\nabla B(t)=\nabla B(0)\left(\frac{t_1 - t_a}{t - t_a}\right)^p \tag{7}$$

in which $\nabla B(0)$ is the initial field gradient, $\nabla B(t)$ is the field gradient at time t, t_1 is a pre-decay period where the field gradient is held constant, t_a is a second time parameter, and p is a number greater than zero. For the experiments reported here, t_1 = 16 minutes, t_a = −40 minutes, and p = 6.

Magnetic Refinement of Drug Carrier Formulation

In this case, the supplied magnetic nanoparticle suspension was diluted 1:2 with Milli-Q water before introduction to the system. Two different initial field gradients were employed, corresponding to 82 mT and 43 mT at the outer channel wall. For these experiments, a 100 μL sample loop was filled with the sonicated suspension. The sample loading was therefore 25 times higher compared to the analytical experimental runs. The sample was carried onto the channel at a loading flow rate of 0.10 mL/min for 3 minutes. A stop flow period of 30 minutes was given for sample relaxation. The carrier fluid flow was then reestablished at 0.50 mL/min. An intense sharply-fronted peak would be detected by the UV-detector due to the elution of weakly retained material. The peak decayed slowly back to the baseline over a period of, typically, around 15 to 20 minutes, corresponding to 8 to 10 channel volumes. The channel was then removed from the quadrupole magnet and the eluent corresponding to a second strong peak collected. The collected volume was typically around 2.5 mL.

For analysis of the collected, refined material by QMgFFF it was necessary to reconcentrate the suspension. This was accomplished by evaporation. The carrier fluid was de-ionized Milli-Q water and the dilution of the material did not introduce any surfactants or salts that could be concentrated by evaporating the water. Evaporation was achieved by blowing a stream of clean, filtered air across the surface of the suspension at room temperature for around 3 hours. The conical base of a 50 mL BD Falcon™ tube was used to contain the sample. The tube was cut at about 0.5 cm above the conical base.

Results

Figure 2 shows the elution profile for a binary fractionation. The first peak corresponds to the fraction of particles that are weakly retained in the channel at the applied field gradient. These particles start to elute almost immediately upon start of the flow of carrier fluid. The peak

exhibits a long tail that extends over about 15 minutes. The tail corresponds to those particles that are retained to some extent at the applied field gradient. Increasing elution time corresponds to greater retention and to greater dilution in the outlet stream. At about 26 minutes, when the particle concentration in the outlet stream had fallen to a relatively low level, the channel was removed from the magnet and the second peak was obtained. This corresponds to the material that was retained in the channel at the initially applied field gradient. This material would be collected for re-concentration by evaporation.

Figure 3 shows the QMgFFF elution curves obtained under conditions of programmed field gradient decay for the original sample and for the refined fraction of the original sample that was retained at a field of 82 mT at the channel wall. The narrow peaks at the start of each elution curve are the void peaks. These are routinely exhibited in FFF fractograms, and correspond to the elution of non retained material. The narrow peaks at the ends of the elution curves are obtained when the channel is removed from the quadrupole magnet. They correspond to strongly retained particles, possibly including aggregates. The dashed line shows the variation of field at the outer channel wall as a function of time (this refers to the right hand axis). The original sample has a peak maximum at around 60 minutes, while the refined fraction has a peak maximum at around 75 minutes. More importantly, the refined fraction is seen to start to elute at a much lower field gradient than the original sample. This is the desired result. It indicates that the original sample has been depleted of lesser magnetic particles.

Figure 4 shows the equivalent results for refinement using a field gradient corresponding to a field of 43 mT at the outer channel wall. In this case, the peak maximum for the refined material lies at about 80 minutes – a little later than for the material refined at 82 mT. This is as expected. To be retained on the channel at 43 mT, the particles must contain more magnetite than those retained at 82 mT. The small shoulder on the leading part of the elution curve is unexpected and was probably an artifact. Note that the heights of the peaks for the refined samples relative to that of the original are not significant. There was no control of the degree of concentration of the refined samples following collection.

The calculated mass distributions in logarithm of equivalent spherical core diameter for the original and refined (at 82 mT and at 43 mT) samples are shown in Figure 5. The transformation is carried out using a computer program based on a general approach to data reduction for FFF.[213] Data reduction takes into account the actual decay of field gradient as calculated from the continuously monitored field at the outer channel wall. It is assumed that particles elute via the ideal mechanism of FFF where there is assumed to be no significant particle-particle interactions. To carry out the transformation, a magnetization curve was assumed. A function was fitted to a typical, published magnetization curve for magnetite nanoparticles.[214] The relationship is given by

$$M = \frac{9.152 \times 10^6 B}{1 + 27.30B - 0.9229 B^2} \quad (8)$$

where M has units of A/m and B units of T. Equation (8) may differ from the magnetization curve for the magnetic nanoparticles incorporated into the drug carriers. The difference however is likely to be very small. Jain et al.[119] measured the magnetization for a batch of the oleic acid-Pluronic-coated nanoparticles and found a magnetization of 59.2 ± 0.8 emu/g of magnetite at a field of 1.2 T. The amount of magnetite was determined from the iron content as measured by atomic absorption spectroscopy, assuming all iron was in the form of magnetite. Equation (8) predicts a magnetization of 64.6 emu/g of magnetite at a field of 1.2 T. (The conversion of units: 1 emu/g = ρ emu/mL = ρ × 10^3 A/m, where ρ is the density of magnetite,

taken to be 5.24 g/mL.) The difference in this case is less than 10%. Figure 6 shows the same data transformed into mass distributions in logarithm of magnetite core mass.

It must be pointed out that no light scattering corrections were applied for the response of the UV-detector, and the mass distribution curves may have some associated error. The differences between mass distribution curves may however reveal useful information. We note that the calculated diameters are far larger than the 11 nm mean iron oxide particle size determined by TEM. This would suggest that many of the iron oxide nanoparticles are incorporated into each of the nanoparticle drug carriers, or that the sample particles are strongly aggregated. We shall return to this point in the Discussion. The polydispersity of the samples is also very high, which also suggests that there is a distribution in the number of 11 nm iron oxide particles incorporated into the cores. The mean core diameter is seen to be increased by the refinement procedure. The more important observation is that the particles containing less magnetite are very strongly depleted in the refined material. The refinement of a magnetic drug targeting formulation in this way would significantly impact the efficiency of drug targeting.

Discussion

The apparent equivalent spherical magnetic core diameters were calculated to be much larger than the 11 nm mean diameter of the iron oxide particles as determined by TEM. This is not surprising. Consider the fact that the refinement procedure retained particles on the channel at field gradients corresponding to 82 mT and 43 mT at the outer channel wall, corresponding to B_o / r_o = 0.082 T / 0.00744 m = 11 T/m, and B_o / r_o = 5.8 T/m, respectively. At a field of 82 mT, the assumed magnetization of magnetite (given by eq (8)) is 230,000 A/m. We would then expect the retention parameter λ, as given by eq (2), to be equal to 9.2 for a particle having a single 11 nm magnetite particle at its core. This is far too large for such a particle to be retained in the channel to any significant degree. For example, a retention ratio of 0.1 corresponds to λ of less than 0.018.

We could speculate that particle dipole-dipole interaction causes particle chaining and aggregation. Rosensweig[215] gives the energy of interaction between two identical spherical magnetized particles as

$$E_{dd}=\frac{\pi}{9}\frac{\mu_0 M^2 d^3}{(1+2)^3} \tag{9}$$

where μ_0 is the magnetic permeability of free space ($\mu_0 = 4\pi\times10^{-7}$ H/m), M is the particle magnetization, d is the particle diameter, and $l = 2s / d$, with s as the surface to surface separation distance. We can transform this equation to give the dipole-dipole interaction energy between two identical core-shell magnetized particles in contact. The shells are assumed to be effectively non-magnetic, and have thickness $s/2$. The overall particle diameter d_p is therefore equal to $d_m + s$, where d_m is the diameter of the cores having magnetization M. The result is given by

$$E_{dd}=\frac{\pi}{72}\frac{\mu_0 M^2 {d_m}^6}{{d_p}^3} \tag{10}$$

For the same conditions of 82 mT and 11 nm cores, and assuming overall mean particle diameters of 193 nm (as determined by dynamic light scattering), we calculate E_{dd} of 7.1×10^{-25} J. Compared to thermal energy kT at 298 K, 4.1×10^{-21} J, this is extremely small. Thermal energy would therefore prevent any aggregation by dipole-dipole interaction.

It is a fact that significant fractions of the magnetic nanoparticles are strongly retained in the channel at the field gradients of 11 and 5.8 T/m. If we assume an ideal FFF mechanism, where there is no particle-particle interaction, we can calculate the minimum core diameter to obtain retention. Suppose we require $R < 0.10$, or $\lambda < 0.018$, at $B_o = 82$ mT and $B_o / r_o = 11$ T/m. Solving eq (2) we obtain the requirement that $d_m > 88$ nm. This is the correct order of magnitude for consistency with Figure 5. The distribution for particles retained in the channel at these conditions extends for somewhere over 100 nm and up. Note that an 88 nm core is equivalent in mass to a core consisting of over 500 of the 11 nm iron oxide nanoparticles.

Suppose we now consider the threshold core diameters for significant dipole-dipole interaction at 82 mT. This is given by equating E_{dd} as calculated by eq (10) with thermal energy kT, assuming d_p of 193 nm. The result is 47 nm, equivalent to a core consisting of 80 of the 11 nm iron oxide nanoparticles. We see that for the conditions under consideration and the mean overall particle size, that the core diameter corresponding to critical dipole-dipole interaction is of the same order of magnitude as the core diameter required for retention according to the ideal FFF mechanism. This is, of course, coincidental.

There is another approach we can take to estimate the size of the cores. Jain et al.[119] reported the mass composition of the drug carrier determined by thermogravimetric analysis (TGA). They were reported to be 70.1 wt% iron oxide, 15.4 wt% oleic acid, and 14.5 wt% Pluronic F-127. An 11 nm sphere of magnetite has a volume of 6.97×10^{-25} m^3, and therefore a mass of 3.65×10^{-18} g. Assuming a single iron oxide nanoparticle occupies the core, the particle must incorporate 8.02×10^{-19} g or 8.96×10^{-25} m^3 of oleic acid (density of 0.895 g/mL). The oleic acid is hydrophobic, and would form a coat with thickness 1.75 nm, having an outer diameter of 14.5 nm. The particle must also include 7.55×10^{-19} g of Pluronic F-127, which has a dry density of 1.05 g/mL. Pluronic F-127 is a triblock co-polymer of poly(ethylene oxide)$_{106}$-poly (propylene oxide)$_{70}$-poly(ethylene oxide)$_{106}$, having a mean molecular weight of 12600. Studies of Pluronic F-127 micelles in water[216] suggest a volume fraction of poly(ethylene oxide) in the corona of 0.15, the remaining 0.85 being water. To take into account that only the two end-chains occupy the corona, we can estimate the Pluronic as being present at an overall volume fraction of 0.20, and its volume including the water component would then be 3.60×10^{-24} m^3, giving a total particle volume of 5.19×10^{-24} m^3. This corresponds to a particle diameter of just 21.5 nm, while the measured mean hydrodynamic diameter by dynamic light scattering was 193 nm. This is a discrepancy that amounts to a factor of 9.0 in diameter or 720 in volume. This would indicate a core diameter of 99 nm, and a core mass of 2.6×10^{-6} ng.

We can consider the expected coating thickness for Pluronic F-127. Lin and Alexandridis[217] carried out dynamic light scattering studies of carbon black (CB) nanoparticles and CB particles coated with Pluronic F-127. The CB particles had a mean diameter of 104 nm. In a 1% Pluronic F-127 solution at room temperature, their mean diameters were measured to be 142.5 nm. The Pluronic coating was therefore 19 nm thick. Our calculations based on composition by weight, and a single 11 nm iron oxide core particle, suggested a Pluronic coating of only 3.5 nm thickness. If we assume that the Pluronic forms a coating of 19 nm thickness and adjust the quantities of the other components in the particle in proportion, the overall particle diameter would be 117 nm. This is much more in agreement with the 193 nm dynamic light scattering result. The volume discrepancy amounts to a factor of 160. This would suggest a core containing 160 of the 11 nm iron oxide nanoparticles.

The effectiveness of the refinement approach is most clearly shown by the results in Figure 6. Even if we do not assume accuracy of the absolute values for core mass, the relative differences in the curves indicate that the particles that interact with the magnetic field the least are strongly depleted by the refinement. There is more than an order of magnitude difference in the core

mass and therefore in the strength of interaction with the field of the smallest core particles of the unrefined and refined materials.

Conclusions

All of the evidence suggests that the drug carriers are much more strongly magnetic than would be expected if their cores were composed of single 11 nm iron oxide nanoparticles. The broad polydispersity could also be attributed to a wide distribution in the number of 11 nm iron oxide particles incorporated into the nanocarriers. The mechanism for particle retention in the FFF channel may not be fully understood. It may be that during analysis using field gradient decay, one obtains a programmed release of particles from interaction with other particles on the wall. However, previous work has demonstrated the extremely good reproducibility of magnetic nanoparticle elution under programmed field gradient conditions.[206] The release would have to occur in an extremely reproducible way. An interesting observation regards the very fast release of the retained material on removal of the channel from the quadrupole field. No stopped flow period was required for the secondary relaxation to occur. The retained material was resuspended into the carrier fluid and swept from the channel by passage of only about 3 channel volumes.

The elution profiles for the refined and unrefined magnetic nanoparticles indicate that the samples are indeed depleted of the less magnetic fractions using the procedure described in this manuscript. Whatever the mechanism of particle retention, the observed retention and elution of the particles from the channel must reflect their behavior in a magnetic field gradient. This behavior is of direct relevance to the magnetic targeting of cytotoxic agents in the body. The refined material starts to elute at lower field gradients than the unrefined material. Lower field gradients would therefore be required to focus the refined material. Also, the depletion of the less magnetic fraction would have the beneficial consequence of reducing systemic toxicity.

The refinement experiments were carried out using samples of 100 μL. As discussed earlier, it should be possible to load sample volumes exceeding the channel volume. Experiments are planned to explore the loading capacity of the current channel while obtaining the desired refinement. Experiments are also planned in which both the retained and non retained fractions will be analyzed by QMgFFF and dynamic light scattering.

Acknowledgment

The authors thank the National Institutes of Health for financial support from grant R01 CA62349, and the National Science Foundation from grant CTS-0125657. The authors also thank Dr. Tapan Jain for preparing the magnetic nanoparticle material in the laboratory of Dr. Vinod Labhasetwar, Department of Biomedical Engineering, Cleveland Clinic.

References

1. Freeman MW, Arrott A, Watson JHL. Magnetism in medicine. J. Appl. Phys 1960;5:S404–S405.
2. Meyers PH, Cronic F, Nice CM Jr. Experimental approach in the use of magnetic control of metallic iron particles in the lymphatic and vascular system of dogs as a contrast and isotopic agent. Am. J. Roentgenol. Radium Ther. Nucl. Med 1963;90:1068–1077.
3. Meyers PH, Nice CM Jr, Meckstroth GR, Becker HC, Moser PJ, Goldstein M. Pathological studies following magnetic control of metallic iron particles in the lymphatic and vascular system of dogs as a contrast and isotropic agent. Am. J. Roentgenol. Radium Ther. Nucl. Med 1966;96(4):913–921.
4. Nakamura T, Konno K, Moroné T, Tsuya N, Hatano M. Magneto-medicine: Biological aspects of ferromagnetic fine particles. J. Appl. Phys 1971;42(4):1320–1324.

5. Gupta PK, Hung CT. Minireview. Magnetically controlled targeted micro-carrier systems. Life Sci 1989;44(3):175–186. [PubMed: 2644506]
6. Zimmermann U, Pilwat G. Organ specific application of drugs by means of cellular capsule systems. Zeitschrift fur Naturforschung Section C Biosciences 1976;31(11–12):732–736.
7. Zimmermann U, Pilwat G, Vienken J. Erythrocytes and lymphocytes as drug carrier systems: techniques for entrapment of drugs in living cells. Rec. Results Cancer Res 1980;75:252–259.
8. Danilov YN, Rudchenko SA, Samokhin GP, Orekhov AN, Il'ina MB, Makhmudov SY, Dobrova NB, Buyanovskii VL, Pokrovskii AV. Concentration of erythrocyte-based magnetic carriers in the bloodstream. Bull. Exp. Biol. Med 1985;100(6):1684–1686.
9. Orekhova NM, Akchurin RS, Belyaev AA, Smirnov MD, Ragimov SE, Orekhov AN. Local prevention of thrombosis in animal arteries by means of magnetic targeting of aspirin-loaded red cells. Thromb. Res 1990;57(4):611–616. [PubMed: 2326776]
10. Kiwada H, Sato J, Yamada S, Kato Y. Feasibility of magnetic liposomes as a targeting device for drugs. Chem. Pharm. Bull 1986;34(10):4253–4258. [PubMed: 3829157]
11. Ishii F, Takamura A, Ishigami Y. Preparation and characterization of lipid vesicles containing magnetite and an anticancer drug. J. Dispersion Sci. Technol 1990;11(6):581–592.
12. Akimoto M, Morimoto Y. The development of a magnetic emulsion as drug carrier. J. Pharmacobio-Dynamics 1982;5(1):s-15.
13. Akimoto M, Morimoto Y. Use of magnetic emulsion as a novel drug carrier for chemotherapeutic agents. Biomaterials 1983;4(1):49–51. [PubMed: 6838956]
14. Morimoto Y, Subibayashi K, Akimoto M. Magnetic guidance of ferro-colloid-entrapped emulsion for site-specific drug delivery. Chem. Pharm. Bull 1983;31(1):279–285. [PubMed: 6850943]
15. Akimoto M, Sugibayashi K, Morimoto Y. Application of magnetic emulsions for sustained release and targeting of drugs in cancer chemotherapy. J. Controlled Release 1985;1(3):205–215.
16. Mosbach K, Schröder U. Preparation and application of magnetic polymers for targeting of drugs. FEBS Lett 1979;102(1):112–116. [PubMed: 156645]
17. Schroder U, Mosbach K. Magnetic microspheres for targeting of drugs. Appl. Biochem. Biotechnol 1982;7(1–2):63–65.
18. Widder KJ, Senyei AE, Scarpelli DG. Magnetic microspheres: a model system of site specific drug delivery in vivo. Proc. Soc. Exp. Biol. Med 1978;158(2):141–146. [PubMed: 674215]
19. Senyei A, Widder K, Czerlinski G. Magnetic guidance of drug-carrying microspheres. J. Appl. Phys 1978;49(6):3578–3583.
20. Widder K, Flouret G, Senyei A. Magnetic microspheres: Synthesis of a novel parenteral drug carrier. J. Pharm. Sci 1979;68(1):79–82. [PubMed: 569198]
21. Widder KJ, Senyei AE, Ranney DF. Magnetically responsive microspheres and other carriers for the biophysical targeting of antitumor agents. Adv. Pharmacol. Chemother 1979;16:213–271. [PubMed: 382799]
22. Widder KJ, Morris RM, Poore G, Howard DP, Senyei AE. Tumor remission in Yoshida sarcoma-bearing rats by selective targeting of magnetic albumin microspheres containing doxorubicin. Proc. Natl. Acad. Sci. U.S.A 1981;78(1):579–581. [PubMed: 6941258]
23. Senyei AE, Reich SD, Gonczy C, Widder KJ. *In vivo* kinetics of magnetically targeted low-dose doxorubicin. J. Pharm. Sci 1981;70(4):389–391. [PubMed: 7229949]
24. Senyei AE, Widder KJ. Drug targeting: Magnetically responsive albumin microspheres--A review of the system to date. Gynicol. Oncol 1981;12(1):1–13.
25. Widder KJ, Morris RM, Poore GA, Howard DP, Senyei AE. Selective targeting of magnetic albumin microspheres containing low-dose doxorubicin: Total remission in Yoshida sarcoma-bearing rats. Eur. J. Cancer Clin. Oncol 1983;19(1):135–139. [PubMed: 6682771]
26. Widder KJ, Marino PA, Morris RM, Howard DP, Poore GA, Senyei AE. Selective targeting of magnetic albumin microspheres to the Yoshida sarcoma: Ultrastructural evaluation of microsphere disposition. Eur. J. Cancer Clin. Oncol 1983;19(1):141–147. [PubMed: 6682772]
27. Widder KJ, Senyei AE. Magnetic microspheres: a vehicle for selective targeting of drugs. Pharmacol. Therap 1983;20(3):377–395. [PubMed: 6351115]

28. Driscoll CF, Morris RM, Senyei AE, Widder KJ, Heller GS. Magnetic targeting of microspheres in blood flow. Microvasc. Res 1984;27(3):353–369. [PubMed: 6727704]
29. Senyei AE, Driscoll CF, Widder KJ. Biophysical drug targeting: magnetically responsive albumin microspheres. Methods Enzymol 1985;112:56–67. [PubMed: 4046864]
30. Ranney DF. Targeted modulation of acute inflammation. Science 1985;227(4683):182–184. [PubMed: 3966151]
31. Gupta PK, Morris C, Hung CT. Evaluation of magnetic albumin microspheres for site-specific delivery of adriamycin. Proc. Univ. Otago Med. School 1986;64(3):63–64.
32. Gupta PK, Hung CT, Lam FC, Perrier DG. Albumin microspheres. III. Synthesis and characterization of microspheres containing adriamycin and magnetite. Int. J. Pharm 1988;43(1–2):167–177.
33. Gallo JM, Hung CT, Gupta PK, Perrier DG. Physiological pharmacokinetic model of adriamycin delivered via magnetic albumin microspheres in the rat. J. Pharmacokinetics Biopharm 1989;17(3): 305–326.
34. Gupta PK, Hung C-T, Rao NS. Ultrastructural disposition of adriamycin-associated magnetic albumin microspheres in rats. J. Pharm. Sci 1989;78(4):290–294. [PubMed: 2724092]
35. Gallo JM, Gupta PK, Hung CT, Perrier DG. Evaluation of drug delivery following the administration of magnetic albumin microspheres containing adriamycin to the rat. J. Pharm. Sci 1989;78(3):190–194. [PubMed: 2724075]
36. Gupta PK, Hung C-T. Targeted delivery of low dose doxorubicin hydrochloride administered via magnetic albumin microspheres in rats. J. Microencapsulation 1990;7(1):85–94. [PubMed: 2308056]
37. Gupta PK, Hung CT. Comparative disposition of adriamycin delivered via magnetic albumin microspheres in presence and absence of magnetic field in rats. Life Sci 1990;46(7):471–479. [PubMed: 2304381]
38. Gupta PK, Hung C-T, Albumin microspheres V. Evaluation of parameters controlling the efficacy of magnetic microspheres in the targeted delivery of adriamycin in rats. Int. J. Pharm 1990;59(1): 57–67.
39. Ishii F, Takamura A, Noro S. Magnetic microcapsules for *in vitro* testing as carrier for intravascular administration of anticancer drugs : Preparation and physicochemical properties. Chem. Pharm. Bull 1984;32(2):678–684.
40. Ruuge EK, Rusetski AN. Magnetic fluids as drug carriers: Targeted transport of drugs by a magnetic field. J. Magn. Magn. Mater 1993;122(1–3):335–339.
41. Ovadia H, Paterson PY, Hale JR. Magnetic microspheres as drug carriers: Factors influencing localization at different anatomical sites in rats. Isr. J. Med. Sci 1983;19(7):631–637. [PubMed: 6604045]
42. Hassan EE, Gallo JM. Targeting anticancer drugs to the brain. I: Enhanced brain delivery of oxantrazole following administration in magnetic cationic microspheres. J. Drug Targeting 1993;1 (1):7–14.
43. Devineni D, Klein-Szanto A, Gallo JM. Targeting anticancer drugs to the brain. III: Tissue distribution of methotrexate following administration as a solution and as a magnetic microsphere conjugate in rats bearing brain tumors. J. Neuro-Oncol 1995;24(2):143–152.
44. Häfeli UO, Sweeney SM, Beresford BA, Humm JL, Macklis RM. Effective targeting of magnetic radioactive ^{90}Y-microspheres to tumor cells by an externally applied magnetic field. Preliminary *in vitro* and *in vivo* results. Nucl. Med. Biol 1995;22(2):147–155. [PubMed: 7767307]
45. Pulfer SK, Gallo JM. Enhanced brain tumor selectivity of cationic magnetic polysaccharide microspheres. J. Drug Targeting 1998;6(3):215–228.
46. Schütt W, Grüttner C, Teller J, Westphal F, Häfeli U, Paulke B, Goetz P, Finck W. Biocompatible magnetic polymer carriers for in vivo radionuclide delivery. Artificial Organs 1999;23(1):98–103. [PubMed: 9950186]
47. Richardson, G.; Cummings, LJ.; King, J.; Gaffney, E.; Hazelwood, L.; Chapman, J. Magnetically-targeted drug delivery. Nottingham, Nottingham: 1st Mathematics-in-Medicine Study Group; 2000.
48. Häfeli U, Pauer G, Failing S, Tapolsky G. Radiolabeling of magnetic particles with rhenium-188 for cancer therapy. J. Magn. Magn. Mater 2001;225(1–2):73–78.
49. Johnson J, Kent T, Koda J, Peterson C, Rudge S, Tapolsky G. The MTC technology: A platform technology for the site-specific delivery of pharmaceutical agents. Eur. Cells Mater 2002;3:12–15.

50. Rotariu O, Strachan NJC. Modelling magnetic carrier particle targeting in the tumor microvasculature for cancer treatment. J. Magn. Magn. Mater 2005;293(1):639–646.
51. Grief AD, Richardson G. Mathematical modelling of magnetically targeted drug delivery. J. Magn. Magn. Mater 2005;239(1):455–463.
52. Mishima F, Takeda S-i, Izumi Y, Nishijima S. Three dimensional motion control system of ferromagnetic particles for magnetically targeted drug delivery systems. IEEE Trans. Appl. Supercond 2006;16(2):1539–1542.
53. Furlani EJ, Furlani EP. A model for predicting magnetic targeting of multifunctional particles in the microvasculature. J. Magn. Magn. Mater 2007;312(1):187–193.
54. Gleich B, Hellwig N, Bridell H, Jurgons R, Seliger C, Alexiou C, Wolf B, Weyh T. Design and evaluation of magnetic fields for nanoparticle drug targeting in cancer. IEEE Trans. Nanotechnol 2007;6(2):164–170.
55. Häfeli UO, Gilmour K, Zhou A, Lee S, Hayden ME. Modeling of magnetic bandages for drug targeting: Button vs. Halbach arrays. J. Magn. Magn. Mater 2007;311(1):323–329.
56. Forbes ZG, Yellen BB, Barbee KA, Friedman G. An approach to targeted drug delivery based on uniform magnetic fields. IEEE Trans. Magn 2003;39(5):3372–3377.
57. Iacob G, Rotariu O, Strachan NJC, Häfeli UO. Magnetizable needles and wires - modeling an efficient way to target magnetic microspheres *in vivo*. Biorheology 2004;41(5):599–612. [PubMed: 15477667]
58. Ritter JA, Ebner AD, Daniel KD, Stewart KL. Application of high gradient magnetic separation principles to magnetic drug targeting. J. Magn. Magn. Mater 2004;280(2–3):184–201.
59. Yellen BB, Forbes ZG, Halverson DS, Fridman G, Barbee KA, Chorny M, Levy R, Friedman G. Targeted drug delivery to magnetic implants for therapeutic applications. J. Magn. Magn. Mater 2005;293(1):647–654.
60. Avilés MO, Ebner AD, Chen H, Rosengart AJ, Kaminski MD, Ritter JA. Theoretical analysis of a transdermal ferromagnetic implant for retention of magnetic drug carrier particles. J. Magn. Magn. Mater 2005;293(1):605–615.
61. Avilés MO, Ebner AD, Ritter JA. Ferromagnetic seeding for the magnetic targeting of drugs and radiation in capillary beds. J. Magn. Magn. Mater 2007;310(1):131–144.
62. Chen H, Ebner AD, Rosengart AJ, Kaminski MD, Ritter JA. Analysis of magnetic drug carrier particle capture by a magnetizable intravascular stent: 1. Parametric study with single wire correlation. J. Magn. Magn. Mater 2004;284:181–194.
63. Chen H, Ebner AD, Kaminski MD, Rosengart AJ, Ritter JA. Analysis of magnetic drug carrier particle capture by a magnetizable intravascular stent—2: Parametric study with multi-wire two-dimensional model. J. Magn. Magn. Mater 2005;293(1):616–632.
64. Avilés MO, Chen H, Ebner AD, Rosengart AJ, Kaminski MD, Ritter JA. In vitro study of ferromagnetic stents for implant assisted-magnetic drug targeting. J. Magn. Magn. Mater 2007;311 (1):306–311.
65. Arbab AS, Jordan EK, Wilson LB, Yocum GT, Lewis BK, Frank JA. *In vivo* trafficking and targeted delivery of magnetically labeled stem cells. Human Gene Therapy 2004;15(4):351–360. [PubMed: 15053860]
66. Furlani EP. Analysis of particle transport in a magnetophoretic microsystem. J. Appl. Phys 2006;99 (2):024912.
67. Oberteuffer JA. High gradient magnetic separation. IEEE Trans. Magn 1973;MAG-9(3):303–306.
68. Luborsky FE, Drummond BJ. High gradient magnetic separation: Theory versus experiment. IEEE Trans. Magn 1975;11(6):1696–1700.
69. Cummings DL, Prieve DC, Powers GJ. The motion of small paramagnetic particles in a high gradient magnetic separator. IEEE Trans. Magn 1976;12(5):471–473.
70. Schewe H, Takayasu M, Friedlaender FJ. Observation of particle trajectories in an HGMS single-wire system. IEEE Trans. Magn 1980;16(1):149–154.
71. Friedlaender FJ, Gerber R, Kurz W, Birss RR. Particle motion near and capture on single spheres in HGMS. IEEE Trans. Magn 1981;17(6):2801–2803.

72. Panyam J, Labhasetwar V. Biodegradable nanoparticles for drug and gene delivery to cells and tissue. Adv. Drug Deliv. Rev 2003;55(3):329–347. [PubMed: 12628320]
73. Goodwin S, Peterson C, Hoh C, Bittner C. Targeting and retention of magnetic targeted carriers (MTCs) enhancing intra-arterial chemotherapy. J. Magn. Magn. Mater 1999;194(1–3):132–139.
74. Goodwin SC, Bittner CA, Peterson CL, Wong G. Single-dose toxicity study of hepatic intra-arterial infusion of doxorubicin coupled to a novel magnetically targeted drug carrier. Toxicol. Sci 2001;60 (1):177–183. [PubMed: 11222884]
75. Leakakos T, Ji C, Lawson G, Peterson C, Goodwin S. Intravesical administration of doxorubicin to swine bladder using magnetically targeted carriers. Cancer Chemother. Pharmacol 2003;51(6):445–450. [PubMed: 12802508]
76. Gerlowski LE, Jain RK. Microvascular permeability of normal and neoplastic tissues. Microvasc. Res 1986;31(3):288–305. [PubMed: 2423854]
77. Jain RK. Transport of molecules across tumor vasculature. Cancer Metastasis Rev 1987;6(4):559–593. [PubMed: 3327633]
78. Dvorak HF, Nagy JA, Dvorak JT, Dvorak AM. Identification and characterization of the blood vessels of solid tumors that are leaky to circulating macromolecules. Am. J. Pathol 1988;133(1):95–109. [PubMed: 2459969]
79. Yuan F, Dellian M, Fukumura D, Leunig M, Berk DA, Torchilin VP, Jain RK. Vascular permeability in a human tumor xenograft: Molecular size dependence and cutoff size. Cancer Res 1995;55(17): 3752–3756. [PubMed: 7641188]
80. Hobbs SK, Monsky WL, Yuan F, Robertspar WG, Griffith L, Torchilin VP, Jain RK. Regulation of transport pathways in tumor vessels: Role of tumor type and microenvironment. Proc. Natl. Acad. Sci. U.S.A 1998;95(8):4607–4612. [PubMed: 9539785]
81. Desai MP, Labhasetwar V, Amidon GL, Levy RJ. Gastrointestinal uptake of biodegradable microparticles: Effect of particle size. Pharm. Res 1996;13(12):1838–1845. [PubMed: 8987081]
82. Desai MP, Labhasetwar V, Walter E, Levy RJ, Amidon GL. The mechanism of uptake of biodegradable microparticles in Caco-2 cells is size dependent. Pharm. Res 1997;14(11):1568–1573. [PubMed: 9434276]
83. Zauner W, Farrow NA, Haines AMR. In vitro uptake of polystyrene microspheres: effect of particle size, cell line and cell density. J. Controlled Release 2001;71(1):39–51.
84. Allen TM, Chonn A. Large unilamellar liposomes with low uptake into the reticuloendothelial system. FEBS Lett 1987;223(1):42–46. [PubMed: 3666140]
85. Allen TM, Hansen C, Rutledge J. Liposomes with prolonged circulation times: factors affecting uptake by reticuloendothelial and other tissues. Biochim. Biophys. Acta 1989;981(1):27–35. [PubMed: 2719971]
86. Gabizon A, Papahadjopoulos D. Liposome formulations with prolonged circulation time in blood and enhanced uptake by tumors. Proc. Natl. Acad. Sci. U.S.A 1988;85(18):6949–6953. [PubMed: 3413128]
87. Gabizon A, Price DC, Huberty J, Bresalier RS, Papahadjopoulos D. Effect of liposome composition and other factors on the targeting of liposomes to experimental tumors: Biodistribution and imaging studies. Cancer Res 1990;50(19):6371–6378. [PubMed: 1698120]
88. Allen TM, Everest JM. Effect of liposome size and drug release properties on pharmacokinetics of encapsulated drug in rats. J. Pharmacol. Exp. Ther 1983;226(2):539–544. [PubMed: 6875864]
89. Senior JH. Fate and behavior of liposomes in vivo: A review of controlling factors. Crit. Rev. Therapeut. Drug. Carrier Syst 1987;3(2):123–193.
90. Moghimi SM, Hunter AC, Murray JC. Long-circulating and target-specific nanoparticles: Theory to practice. Pharmacological Reviews 2001;53(2):283–318. [PubMed: 11356986]
91. Torchilin VP. Drug targeting. Eur. J. Pharm. Sci 2000;11:S81–S91. [PubMed: 11033430]
92. Torchilin VP. Multifunctional nanocarriers. Adv. Drug Deliv. Rev 2006;58(14):1532–1555. [PubMed: 17092599]
93. Lübbe AS, Bergemann C, Huhnt W, Fricke T, Riess H, Brock JW, Huhn D. Preclinical experiences with magnetic drug targeting: Tolerance and efficacy. Cancer Res 1996;56(20):4694–4701. [PubMed: 8840986]

94. Lübbe AS, Bergemann C, Riess H, Schriever F, Reichardt P, Possinger K, Matthias M, Dörken B, Herrmann F, Gürtler R, Hohenberger P, Haas N, Sohr R, Sander B, Lemke A-J, Ohlendorf D, Huhnt W, Huhn D. Clinical experiences with magnetic drug targeting: A Phase I study with 4'-Epidoxorubicin in 14 patients with advanced solid tumors. Cancer Res 1996;56(20):4686–4693. [PubMed: 8840985]

95. Gallo, J. M.; Hafeli, U., Correspondence re: A. S. Lübbe et al., Preclinical experiences with magnetic drug targeting: Tolerance and efficacy. Cancer Res., 56: 4694–4701, 1996; and Clinical experiences with magnetic drug targeting: A Phase I study with 4'-epidoxorubicin in 14 patients with advanced solid tumors. Cancer Res., 56: 4686–4693, 1996: Letter. Cancer Res 1997;57(14):3063–3064.3064 [PubMed: 9230223]

96. Lübbe, A. S., Correspondence re: A. S. Lübbe et al., Preclinical Experiences with Magnetic Drug Targeting: Tolerance and Efficacy. Cancer Res., 56: 4694–4701, 1996; and Clinical Experiences with Magnetic Drug Targeting: A Phase I Study with 4'-Epidoxorubicin in 14 Patients with Advanced Solid Tumors. Cancer Res., 56: 4686–4693, 1996 Reply. Cancer Res 1997;57(14):3064–3065.3065

97. Lübbe AS, Bergemann C, Brock J, McClure DG. Physiological aspects in magnetic drug-targeting. J. Magn. Magn. Mater 1999;194(1–3):149–155.

98. Lübbe AS, Alexiou C, Bergemann C. Clinical applications of magnetic drug targeting. J. Surg. Res 2001;95(2):200–206. [PubMed: 11162046]

99. Alexiou C, Arnold W, Klein RJ, Parak FG, Hulin P, Bergemann C, Erhardt W, Wagenpfeil S, Lübbe AS. Locoregional cancer treatment with magnetic drug targeting. Cancer Res 2000;60(23):6641–6648. [PubMed: 11118047]

100. Alexiou C, Arnold W, Hulin P, Klein RJ, Renz H, Parak FG, Bergemann C, Lübbe AS. Magnetic mitoxantrone nanoparticle detection by histology, X-ray and MRI after magnetic tumor targeting. J. Magn. Magn. Mater 2001;225(1–2):187–193.

101. Kubo T, Sugita T, Shimose S, Nitta Y, Ikuta Y, Murakami T. Targeted delivery of anticancer drugs with intravenously administered magnetic liposomes in osteosarcoma-bearing hamsters. Int. J. Oncol 2000;17(2):309–315. [PubMed: 10891540]

102. Kubo T, Sugita T, Shimose S, Nitta Y, Ikuta Y, Murakami T. Targeted systemic chemotherapy using magnetic liposomes with incorporated adriamycin for osteosarcoma in hamsters. Int. J. Oncol 2001;18(1):121–125. [PubMed: 11115548]

103. Nobuto H, Sugita T, Kubo T, Shimose S, Yasunaga Y, Murakami T, Ochi M. Evaluation of systemic chemotherapy with magnetic liposomal doxorubicin and a dipole external electromagnet. Int. J. Cancer 2004;109(4):627–635. [PubMed: 14991586]

104. Pulfer SK, Ciccotto SL, Gallo JM. Distribution of small magnetic particles in brain tumor-bearing rats. J. Neuro-Oncol 1999;41(2):99–105.

105. Mykhaylyk O, Cherchenko A, Ilkin A, Dudchenko N, Ruditsa V, Novoseletz M, Zozulya Y. Glial brain tumor targeting of magnetite nanoparticles in rats. J. Magn. Magn. Mater 2001;225(1–2):241–247.

106. Alexiou C, Schmidt A, Klein R, Hulin P, Bergemann C, Arnold W. Magnetic drug targeting: biodistribution and dependency on magnetic field strength. J. Magn. Magn. Mater 2002;252:363–366.

107. Alexiou C, Jurgons R, Schmid RJ, Bergemann C, Henke J, Erhardt W, Huenges E, Parak F. Magnetic drug targeting - Biodistribution of the magnetic carrier and the chemotherapeutic agent Mitoxantrone after locoregional cancer treatment. J. Drug Targeting 2003;11(3):139–149.

108. Alexiou C, Jurgons R, Schmid R, Hilpert A, Bergemann C, Parak F, Iro H. In vitro and in vivo investigations of targeted chemotherapy with magnetic nanoparticles. J. Magn. Magn. Mater 2005;293(1):389–393.

109. Alexiou C, Diehl D, Henninger P, Iro H, Röckelein R, Schmidt W, Weber H. A high field gradient magnet for magnetic drug targeting. IEEE Trans. Appl. Supercond 2006;16(2):1527–1530.

110. Alexiou C, Schmid RJ, Jurgons R, Kremer M, Wanner G, Bergemann C, Huenges E, Nawroth T, Arnold W, Parak FG. Targeting cancer cells: magnetic nanoparticles as drug carriers. Eur. Biophys. J 2006;35(5):446–450. [PubMed: 16447039]

111. Jurgons R, Seliger C, Hilpert A, Trahms L, Odenbach S, Alexiou C. Drug loaded magnetic nanoparticles for cancer therapy. J. Phys.: Condens. Matter 2006;18(38):S2893–S2902.

112. Wiekhorst F, Seliger C, Jurgons R, Steinhoff U, Eberbeck D, Trahms L, Alexiou C. Quantification of magnetic nanoparticles by magnetorelaxometry and comparison to histology after magnetic drug targeting. J. Nanosci. Nanotechnol 2006;6(9–10):3222–3225. [PubMed: 17048540]

113. Seliger C, Jurgons R, Wiekhorst F, Eberbeck D, Trahms L, Iro H, Alexiou C. In vitro investigation of the behaviour of magnetic particles by a circulating artery model. J. Magn. Magn. Mater 2007;311 (1):358–362.

114. Berry CC, Curtis ASG. Functionalisation of magnetic nanoparticles for applications in biomedicine. J. Phys. D: Appl. Phys 2003;36(13):R198–R206.

115. Berry CC, Wells S, Charles S, Aitchison G, Curtis ASG. Cell response to dextran-derivatised iron oxide nanoparticles post internalisation. Biomaterials 2004;25(23):5405–5413. [PubMed: 15130725]

116. Lemke A-J, Senfft von Pilsach M-I, Lübbe A, Bergemann C, Riess H, Felix R. MRI after magnetic drug targeting in patients with advanced solid malignant tumors. Eur. Radiol 2004;14(11):1949–1955. [PubMed: 15300401]

117. Asmatulu R, Zalich MA, Claus RO, Riffle JS. Synthesis, characterization and targeting of biodegradable magnetic nanocomposite particles by external magnetic fields. J. Magn. Magn. Mater 2005;292:108–119.

118. Gupta AK, Gupta M. Synthesis and surface engineering of iron oxide nanoparticles for biomedical applications. Biomaterials 2005;26(18):3995–4021. [PubMed: 15626447]

119. Jain TK, Morales MA, Sahoo SK, Leslie-Pelecky DL, Labhasetwar V. Iron oxide nanoparticles for sustained delivery of anticancer agents. Mol. Pharm 2005;2(3):194–205. [PubMed: 15934780]

120. Morales MA, Jain TK, Labhasetwar V, Leslie-Pelecky DL. Magnetic studies of iron oxide nanoparticles coated with oleic acid and Pluronic® block copolymer. J. Appl. Phys 2005;97(10): 10Q905.

121. Morishita N, Nakagami H, Morishita R, Takeda S-i, Mishima F, BungoTerazono, Nishijima S, Kaneda Y, Tanaka N. Magnetic nanoparticles with surface modification enhanced gene delivery of HVJ-E vector. Biochem. Biophys. Res. Commun 2005;334(4):1121–1126. [PubMed: 16134237]

122. Mykhaylyk O, Dudchenko N, Dudchenko A. Doxorubicin magnetic conjugate targeting upon intravenous injection into mice: High gradient magnetic field inhibits the clearance of nanoparticles from the blood. J. Magn. Magn. Mater 2005;293(1):473–482.

123. Neuberger T, Schöpf B, Hofmann H, Hofmann M, von Rechenberg B. Superparamagnetic nanoparticles for biomedical applications: Possibilities and limitations of a new drug delivery system. J. Magn. Magn. Mater 2005;293(1):483–496.

124. Rosengart AJ, Kaminski MD, Chen H, Caviness PL, Ebner AD, Ritter JA. Magnetizable implants and functionalized magnetic carriers: A novel approach for noninvasive yet targeted drug delivery. J. Magn. Magn. Mater 2005;293(1):633–638.

125. Son SJ, Reichel J, He B, Schuchman M, Lee SB. Magnetic nanotubes for magnetic-field-assisted bioseparation, biointeraction, and drug delivery. J. Am. Chem. Soc 2005;127(20):7316–7317. [PubMed: 15898772]

126. Tanaka H, Sugita T, Yasunaga Y, Shimose S, Deie M, Kubo T, Murakami T, Ochi M. Efficiency of magnetic liposomal transforming growth factor-beta 1 in the repair of articular cartilage defects in a rabbit model. J. Biomed. Mater. Res. A 2005;73A(3):255–263. [PubMed: 15800858]

127. Xu H, Song T, Bao X, Hu L. Site-directed research of magnetic nanoparticles in magnetic drug targeting. J. Magn. Magn. Mater 2005;293(1):514–519.

128. Zebli B, Susha AS, Sukhorukov GB, Rogach AL, Parak WJ. Magnetic targeting and cellular uptake of polymer microcapsules simultaneously functionalized with magnetic and luminescent nanocrystals. Langmuir 2005;21(10):4262–4265. [PubMed: 16032831]

129. Arruebo M, Galán M, Navascués N, Téllez C, Marquina C, Ibarra MR, Santamaría J. Development of magnetic nanostructured silica-based materials as potential vectors for drug-delivery applications. Chem. Mater 2006;18(7):1911–1919.

130. Chen J, Wu H, Han D, Xie C. Using anti-VEGF McAb and magnetic nanoparticles as double-targeting vector for the radioimmunotherapy of liver cancer. Cancer Lett 2006;231(2):169–175. [PubMed: 16399221]

131. Furlani EP, Ng KC. Analytical model of magnetic nanoparticle transport and capture in the microvasculature. Phys. Rev. E 2006;73(6):061919–061928.

132. Furlani EP, Sahoo Y. Analytical model for the magnetic field and force in a magnetophoretic microsystem. J. Phys. D: Appl. Phys 2006;39(9):1724–1732.

133. Gould P. Nanomagnetism shows *in vivo* potential. Nanotoday 2006;1(4):34–39.

134. Kim M-C, Kim D-K, Lee S-H, Amin MS, Park I-H, Kim C-J, Zahn M. Dynamic characteristics of superparamagnetic iron oxide nanoparticles in a viscous fluid under an external magnetic field. IEEE Trans. Magn 2006;42(4):979–982.

135. Kuhn SJ, Hallahan DE, Giorgio TD. Characterization of superparamagnetic nanoparticle interactions with extracellular matrix in an *in vitro* system. Ann. Biomed. Eng 2006;34(1):51–58. [PubMed: 16477503]

136. Mondalek FG, Zhang YY, Kropp B, Kopke RD, Ge X, Jackson RL, Dormer KJ. The permeability of SPION over an artificial three-layer membrane is enhanced by external magnetic field. J. Nanobiotechnol 2006;4:4.

137. Sunderland CJ, Steiert M, Talmadge JE, Derfus AM, Barry SE. Targeted nanoparticles for detecting and treating cancer. Drug Dev. Res 2006;67(1):70–93.

138. Arruebo M, Fernández-Pacheco R, Ibarra MR, Santamaría J. Magnetic nanoparticles for drug delivery. Nanotoday 2007;2(3):22–32.

139. Dandamudi S, Campbell RB. Development and characterization of magnetic cationic liposomes for targeting tumor microvasculature. Biochim. Biophys. Acta 2007;1768(3):427–438. [PubMed: 17258172]

140. Fernández-Pacheco R, Marquina C, Valdivia JG, Gutiérrez M, Romero MS, Cornudella R, Laborda A, Viloria A, Higuera T, García A, García de Jalónd JA, Ibarra MR. Magnetic nanoparticles for local drug delivery using magnetic implants. J. Magn. Magn. Mater 2007;311(1):318–322.

141. Ibarra MR, Fernandez-Pacheco R, Valdivia JG, Marquina C, Gutiérrez M. Magnetic nanoparticle complexes for drug delivery, and implanted magnets for targeting. AIP Conf. Proc 2007;898:99–105.

142. Klostergaard J, Bankson J, Auzenne E, Gibson D, Yuill W, Seeney CE. Magnetic vectoring of magnetically responsive nanoparticles within the murine peritoneum. J. Magn. Magn. Mater 2007;311(1):330–335.

143. Li W, Nesselmann C, Zhou Z, Ong L-L, Öri F, Tang G, Kaminski A, Lützow K, Lendlein A, Liebold A, Stamm C, Wang J, Steinhoff G, Ma N. Gene delivery to the heart by magnetic nanobeads. J. Magn. Magn. Mater 2007;311(1):336–341.

144. Ma Y-H, Hsu Y-W, Chang Y-J, Hua M-Y, Chen J-P, Wu T. Intra-arterial application of magnetic nanoparticles for targeted thrombolytic therapy: A rat embolic model. J. Magn. Magn. Mater 2007;311(1):342–346.

145. Okassa LN, Marchais H, Douziech-Eyrolles L, Hervé K, Cohen-Jonathan S, Munnier E, Soucé M, Linassier C, Dubois P, Chourp I. Optimization of iron oxide nanoparticles encapsulation within poly(d,l-lactide-co-glycolide) sub-micron particles. Eur. J. Pharm. Biopharm 2007;67(1):31–38. [PubMed: 17289360]

146. Rivière C, Martina M-S, Tomita Y, Wilhelm C, Dinh AT, Ménager C, Pinard E, Lesieur S, Gazeau F, Seylaz J. Magnetic targeting of nanometric magnetic fluid-loaded liposomes to specific brain intravascular areas: A dynamic imaging study in mice. Radiology 2007;244(2):439–448. [PubMed: 17562813]

147. Takeda S-I, Mishima F, Fujimoto S, Izumi Y, Nishijima S. Development of magnetically targeted drug delivery system using superconducting magnet. J. Magn. Magn. Mater 2007;311(1):367–371.

148. Wu T, Hua M-Y, Chen J-p, Wei K-C, Jung SM, Chang Y-J, Jou M-J, Ma Y-H. Effects of external magnetic field on biodistribution of nanoparticles: A histological study. J. Magn. Magn. Mater 2007;311(1):372–375.

149. Pankhurst QA, Connolly J, Jones SK, Dobson J. Applications of magnetic nanoparticles in biomedicine. J. Phys. D: Appl. Phys 2003;36(13):R167–R181.

150. Sahoo SK, Labhasetwar V. Nanotech approaches to drug delivery and imaging. Drug Discovery Today 2003;8(24):1112–1120. [PubMed: 14678737]

151. Fahmya TM, Fonga PM, Goyalb A, Saltzman WM. Targeted for drug delivery. Mater. Today 2005;8:18–26.
152. Ferrari M. Cancer nanotechnology: opportunities and challenges. Nat. Rev. Cancer 2005;5(3):161–171. [PubMed: 15738981]
153. Ferrari M. Nanovector therapeutics. Curr. Opin. Chem. Biol 2005;9(4):343–346. [PubMed: 15967706]
154. Labhasetwar V. Nanotechnology for drug and gene therapy: the importance of understanding molecular mechanisms of delivery. Curr. Opin. Biotechnol 2005;16(6):674–680. [PubMed: 16263259]
155. Vasir JK, Labhasetwar V. Targeted drug delivery in cancer therapy. Technol. Cancer Res. Treat 2005;4(4):363–374. [PubMed: 16029056]
156. Vasir JK, Reddy MK, Labhasetwar VD. Nanosystems in drug targeting: opportunities and challenges. Curr. Nanosci 2005;1(1):47–64.
157. Darton NJ, Hallmark B, Han X, Palit S, Slater NKH, Mackley MR. The in-flow capture of superparamagnetic nanoparticles for targeting therapeutics. Nanomedicine: Nanotechnology, Biology, and Medicine 2008;4(1):19–29.
158. Takayasu M, Gerber R, Friedlaender FJ. Magnetic separation of submicron particles. IEEE Trans. Magn 1983;MAG-19(5):2112–2114.
159. Gerber R, Takayasu M, Friedlaender FJ. Generalization of HGMS theory: The capture of ultra-fine particles. IEEE Trans. Magn 1983;MAG-19(5):2115–2117.
160. Gerber R. Magnetic filtration of ultra-fine particles. IEEE Trans. Magn 1984;MAG-20(5):1159–1164.
161. Kramer AJ, Janssen JJM, Perenboom JAAJ. Single-wire HGMS of colloidal particles: the evolution of concentration profiles. IEEE Trans. Magn 1990;26(5):1858–1860.
162. Moeser GD, Roach KA, Green WH, Hatton TA, Laibinis PE. High-gradient magnetic separation of coated magnetic nanoparticles. AlChE J 2004;50(11):2835–2848.
163. Cotten GB, Eldredge HB. Nanolevel magnetic separation model considering flow limitations. Sep. Sci. Technol 2002;37(16):3755–3779.
164. Ebner AD, Ritter JA, Ploehn HJ. Feasibility and limitations of nanolevel high gradient magnetic separation. Sep. Purif. Technol 1997;11(3):199–210.
165. Giddings JC. A new separation concept based on a coupling of concentration and flow nonuniformities. Sep. Sci 1966;1(1):123–125.
166. Thompson GH, Myers MN, Giddings JC. An observation of a field-flow fractionation effect with polystyrene samples. Sep. Sci 1967;2(6):797–900.
167. Giddings JC. Field-flow fractionation: Analysis of macromolecular, colloidal, and particulate. Science 1993;260(5113):1456–1465. [PubMed: 8502990]
168. Schimpf, ME.; Caldwell, K.; Giddings, JC. Field-Flow Fractionation Handbook. New York, NY: John Wiley & Sons, Inc.; 2000.
169. Giddings JC. A system based on split-flow lateral-transport thin (SPLITT) separation cells for rapid and continuous particle fractionation. Sep. Sci. Technol 1985;20(910):749–768.
170. Springston SR, Myers MN, Giddings JC. Continuous particle fractionation based on gravitational sedimentation in split-flow thin cells. Anal. Chem 1987;59(2):344–350.
171. Gao Y, Myers MN, Barman BN, Giddings JC. Continuous fractionation of glass microspheres by gravitational sedimentation in split-flow thin (SPLITT) cells. Part. Sci. Technol 1991;9(3–4):105–118.
172. Giddings JC. Optimization of transport-driven continuous SPLITT fractionation. Sep. Sci. Technol 1992;27(11):1489–1504.
173. Berg HC, Purcell EM, Stewart WW. A method for separating according to mass a mixture of macromolecules or small particles suspended in a fluid, II. Experiments in a gravitational field. Proc. Natl. Acad. Sci 1967;58(4):1286–1291. [PubMed: 5237862]
174. Giddings JC, Myers MN. Steric field-flow fractionation: A new method for separating 1 to 100 μm particles. Sep. Sci. Technol 1978;13(8):637–645.

175. Giddings JC, Myers MN, Caldwell KD, Pav JW. Steric field-flow fractionation as a tool for the size characterization of chromatographic supports. J. Chromatogr 1979;185:261–271.

176. Thompson GH, Myers MN, Giddings JC. Thermal field-flow fractionation of polystyrene samples. Anal. Chem 1969;41(10):1219–1222.

177. Hovingh ME, Thompson GH, Giddings JC. Column parameters in thermal field-flow fractionation. Anal. Chem 1970;42(2):195–203.

178. Giddings JC, Martin M, Myers MN. High-speed polymer separations by thermal field-flow fractionation. J. Chromatogr 1978;158:419–435.

179. Caldwell KD, Kesner LF, Myers MN, Giddings JC. Electrical field-flow fractionation of proteins. Science 1972;176(4032):296–298. [PubMed: 4111950]

180. Caldwell KD, Gao Y-S. Electrical field-flow fractionation in particle separation. 1. Monodisperse standards. Anal. Chem 1993;65(13):1764–1772. [PubMed: 8368528]

181. Giddings JC, Yang FJF, Myers MN. Flow field-flow fractionation: A versatile new separation method. Science 1976;193(4259):1244–1245. [PubMed: 959835]

182. Giddings JC, Yang FJ, Myers MN. Theoretical and experimental characterization of flow field-flow fractionation. Anal. Chem 1976;48(8):1126–1132.

183. Giddings JC, Yang FJF, Myers MN. Sedimentation field-flow fractionation. Anal. Chem 1974;46 (13):1917–1924.

184. Jönsson JÅ, Carlshaf A. Flow field flow fractionation in hollow cylindrical fibers. Anal. Chem 1989;61(1):11–18.

185. Wijnhoven JEGJ, Koorn JP, Poppe H, Kok WT. Hollow-fibre flow field-flow fractionation of polystyrene sulphonates. J. Chromatogr. A 1995;699(1–2):119–129.

186. Reschiglian P, Roda B, Zattoni A, Min BR, Moon MH. High performance, disposable hollow fiber flow field-flow fractionation for bacteria and cells. First application to deactivated *Vibrio cholerae*. J. Sep. Sci 2002;25(8):490–498.

187. Vickrey TM, Garcia-Ramirez JA. Magnetic field-flow fractionation: theoretical basis. Sep. Sci. Technol 1980;15(6):1297–1304.

188. Mori S. Magnetic field-flow fractionation using capillary tubing. Chromatographia 1986;21(11): 642–644.

189. Latham AH, Freitas RS, Schiffer P, Williams ME. Capillary magnetic field flow fractionation and analysis of magnetic nanoparticles. Anal. Chem 2005;77(15):5055–5062. [PubMed: 16053322]

190. Giddings, JC. The field-flow fractionation family: Underlying principles. In: Schimpf, ME.; Caldwell, K.; Giddings, JC., editors. Field-Flow Fractionation Handbook. New York, NY: John Wiley & Sons; 2000. p. 3-30.

191. Schunk TC, Gorse J, Burke MF. Parameters affecting magnetic field-flow fractionation of metal oxide particles. Sep. Sci. Technol 1984;19(10):653–666.

192. Gorse J, Schunk TC, Burke MF. The study of liquid suspensions of iron oxide particles with a magnetic field-flow fractionation device. Sep. Sci. Technol 1984–85;19(13–15):1073–1085.

193. Semenov SN, Kuznetsov AA. Flow fractionation in a transverse high-gradient magnetic field. Russ. J. Phys. Chem 1986;60(2):247–250.

194. Semenov SN. Flow fractionation in a strong transverse magnetic field. Russ. J. Phys. Chem 1986;60 (5):729–731.

195. Ohara, T.; Mori, S.; Oda, Y.; Yamamoto, K.; Wada, Y.; Tsukamoto, O. Fourth International Symposium on Field-Flow Fractionation (FFF94). Lund, Sweden: 1994. FFF using high gradient and high intensity magnetic field: process analysis.

196. Tsukamoto O, Ohizumi T, Ohara T, Mori S, Wada Y. Feasibility study on separation of several tens nanometer scale particles by magnetic field-flow-fractionation technique using superconducting magnet. IEEE Trans. Appl. Supercond 1995;5(2 Part 1):311–314.

197. Ohara T, Mori S, Oda Y, Wada Y, Tsukamoto O. Feasibility of using magnetic chromatography for ultra-fine particle separation. Proc. IEE Jpn.-Power & Energy 1995:161–166.

198. Ohara T, Mori S, Oda Y, Wada Y, Tsukamoto O. Feasibility of magnetic chromatography for ultra-fine particle separation. Trans. IEE Jpn 1996;116-B(8):979–986.

199. Wang X, Ohara T, Whitby ER, Karki KC, Winstead CH. Computer simulation of magnetic chromatography system for ultra-fine particle separation. Trans. IEE Jpn 1977;117-B(11):1466–1474.

200. Ohara, T. Feasibility of using magnetic chromatography for ultra-fine particle separation. In: Schneider-Muntau, HJ., editor. High Magnetic Fields Applications, Generations, Materials. New Jersey: World Scientific; 1997. p. 43-55.

201. Ohara T, Wang X, Wada H, Whitby ER. Magnetic chromatography: Numerical analysis in the case of particle size distribution. Trans. IEE Jpn 2000;120-A(1):62–67.

202. Karki KC, Whitby ER, Patankar SV, Winstead C, Ohara T, Wang X. A numerical model for magnetic chromatography. Appl. Math. Mod 2001;25(5):355–373.

203. Mitsuhashi K, Yoshizaki R, Ohara T, Matsumoto F, Nagai H, Wada H. Retention of ions in a magnetic chromatograph using high-intensity and high-gradient magnetic fields. Sep. Sci. Technol 2002;37(16):3635–3645.

204. Berthier, J.; Pham, P.; Massé, P. Numerical modeling of magnetic field flow fractionation in microchannels: A two-fold approach using particle trajectories and concentration; International Conference on Modeling and Simulation of Microsystems; Hilton Head Island, South Carolina, USA, Hilton Head Island, South Carolina, USA,. 2001. p. 202-205.

205. Williams PS, Moore LR, Chalmers JJ, Zborowski M. The potential of quadrupole magnetic field-flow fractionation for determining particle magnetization distributions. Eur. Cells Mater 2002;3:203–205.

206. Carpino F, Moore LR, Chalmers JJ, Zborowski M, Williams PS. Quadrupole magnetic field-flow fractionation for the analysis of magnetic nanoparticles. J. Phys.: Conf. Ser 2005;17:174–180.

207. Carpino F, Moore LR, Zborowski M, Chalmers JJ, Williams PS. Analysis of magnetic nanoparticles using quadrupole magnetic field-flow fractionation. J. Magn. Magn. Mater 2005;293(1):546–552.

208. Carpino F, Zborowski M, Williams PS. Quadrupole magnetic field-flow fractionation: A novel technique for the characterization of magnetic nanoparticles. J. Magn. Magn. Mater 2007;311(1): 383–387.

209. Williams PS, Carpino F, Zborowski M. Theory for nanoparticle retention time in the helical channel of quadrupole magnetic field-flow fractionation. J. Magn. Magn. Mater 2009;321(10):1446–1451.

210. Jain TK, Reddy MK, Morales MA, Leslie-Pelecky DL, Labhasetwar V. Biodistribution, clearance, and biocompatibility of iron oxide magnetic nanoparticles in rats. Mol. Pharm 2008;5(2):316–327. [PubMed: 18217714]

211. Jain TK, Richey J, Strand M, Leslie-Pelecky DL, Flask CA, Labhasetwar V. Magnetic nanoparticles with dual functional properties: Drug delivery and magnetic resonance imaging. Biomaterials 2008;29(29):4012–4021. [PubMed: 18649936]

212. Williams PS, Giddings JC. Power programmed field-flow fractionation: A new program form for improved uniformity of fractionating power. Anal. Chem 1987;59(17):2038–2044. [PubMed: 3674422]

213. Williams PS, Giddings MC, Giddings JC. A data analysis algorithm for programmed field-flow fractionation. Anal. Chem 2001;73(17):4202–4211. [PubMed: 11569810]

214. Yamaura M, Camilo RL, Sampaio LC, Macêdo MA, Nakamura M, Toma HE. Preparation and characterization of (3-aminopropyl) triethoxysilane-coated magnetite nanoparticles. J. Magn. Magn. Mater 2004;279(2–3):210–217.

215. Rosensweig, RE. Ferrohydrodynamics. Mineola, NY: Dover Publications, Inc.; 1997.

216. Kurumada, K-i; Robinson, BH. Viscosity studies of pluronic F127 in aqueous solution. Prog. Colloid Polym. Sci 2004;123:12–15.

217. Lin Y, Alexandridis P. Temperature-dependent adsorption of Pluronic F127 block copolymers onto carbon black particles dispersed in aqueous media. J. Phys. Chem. B 2002;106(42):10834–10844.

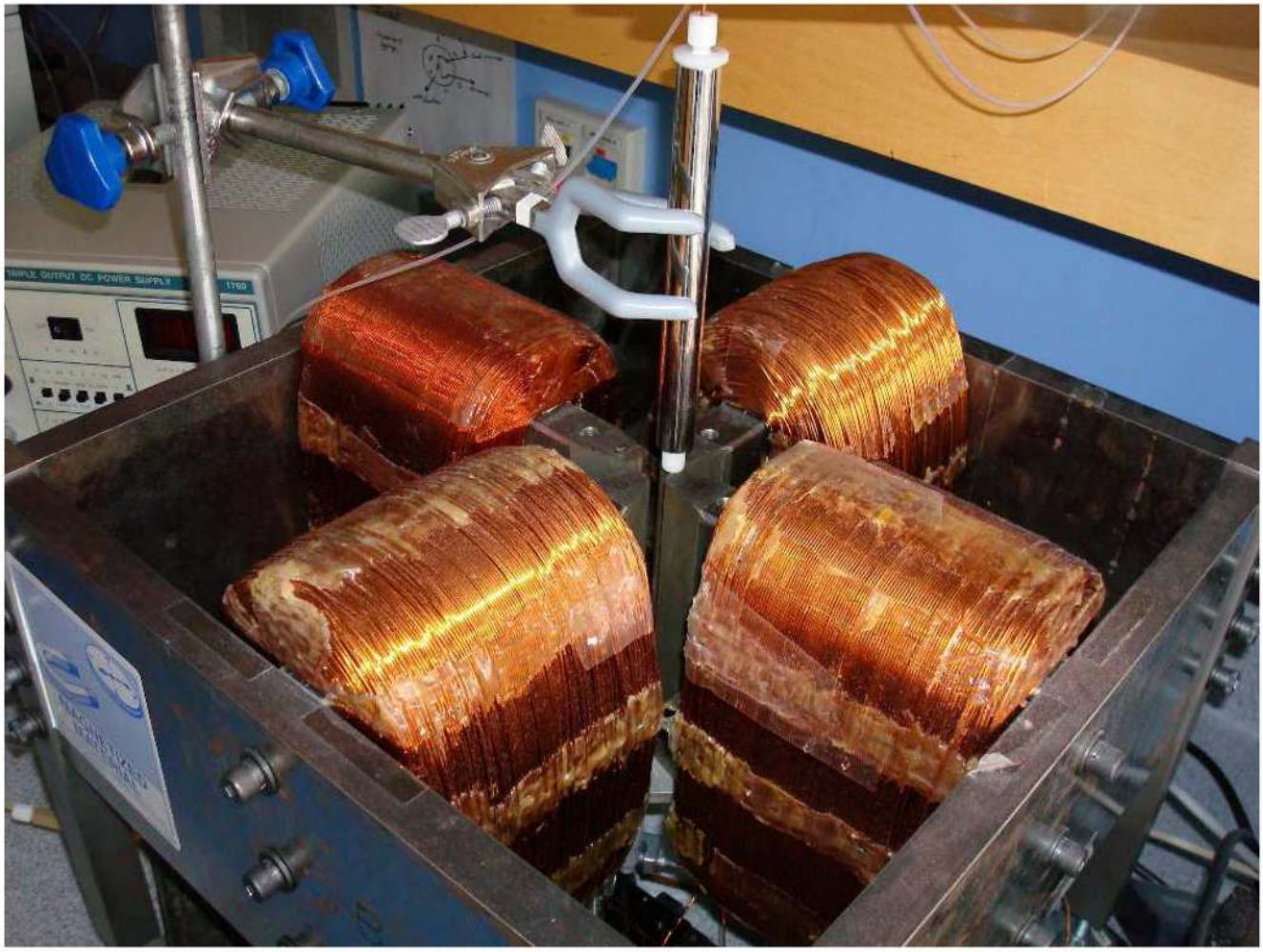

Figure 1.
The quadrupole electromagnet of the field-flow fractionation system. The helical channel, held above the magnet in the photograph, is lowered into the quadrupole aperture below for particle analysis.

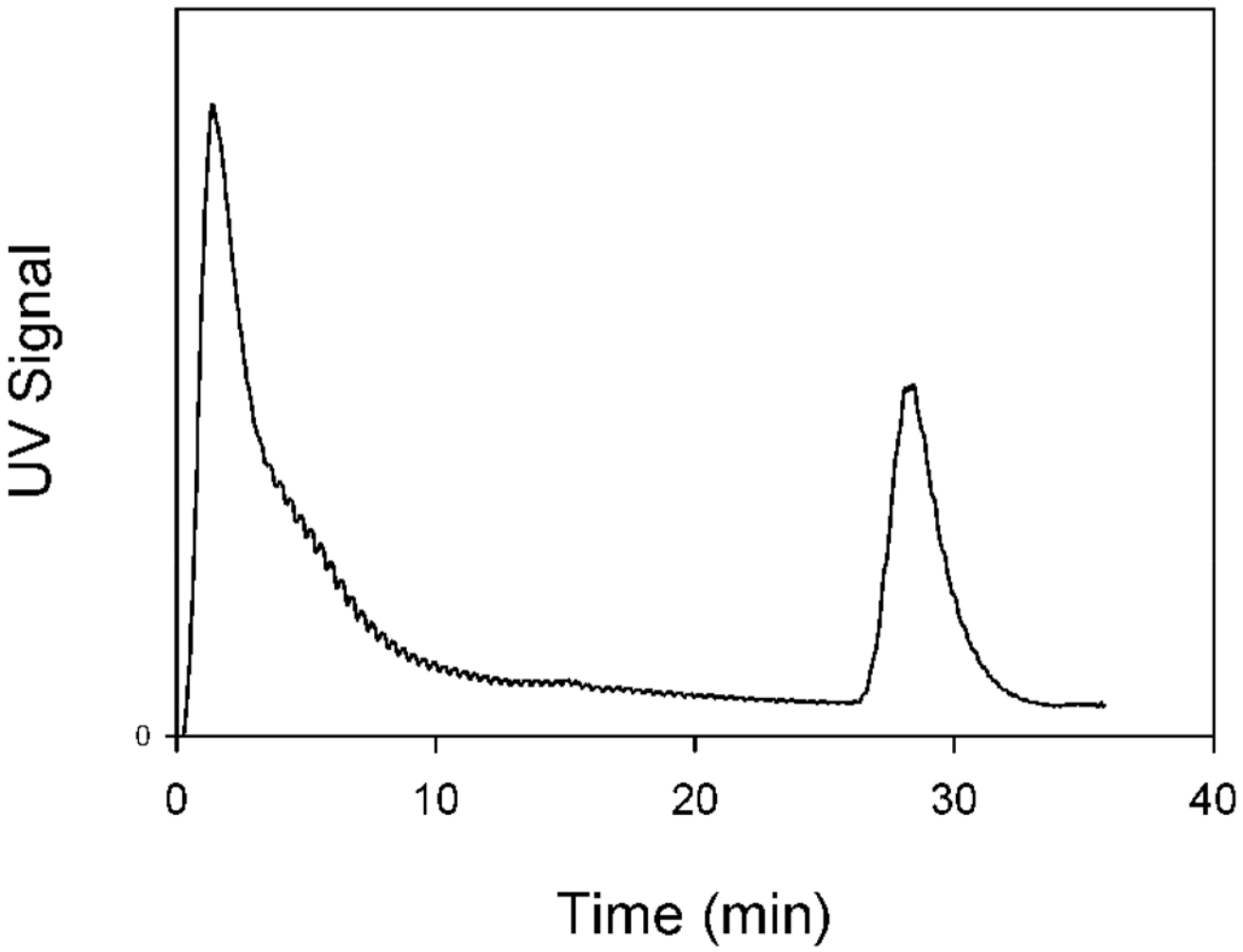

Figure 2.
Binary fractionation of the magnetic nanoparticle sample. The first peak is eluted at the initial magnetic field gradient and corresponds to the less magnetic fraction. The second peak is obtained when the channel is removed from the aperture of the quadrupole magnet, and corresponds to the more magnetic fraction.

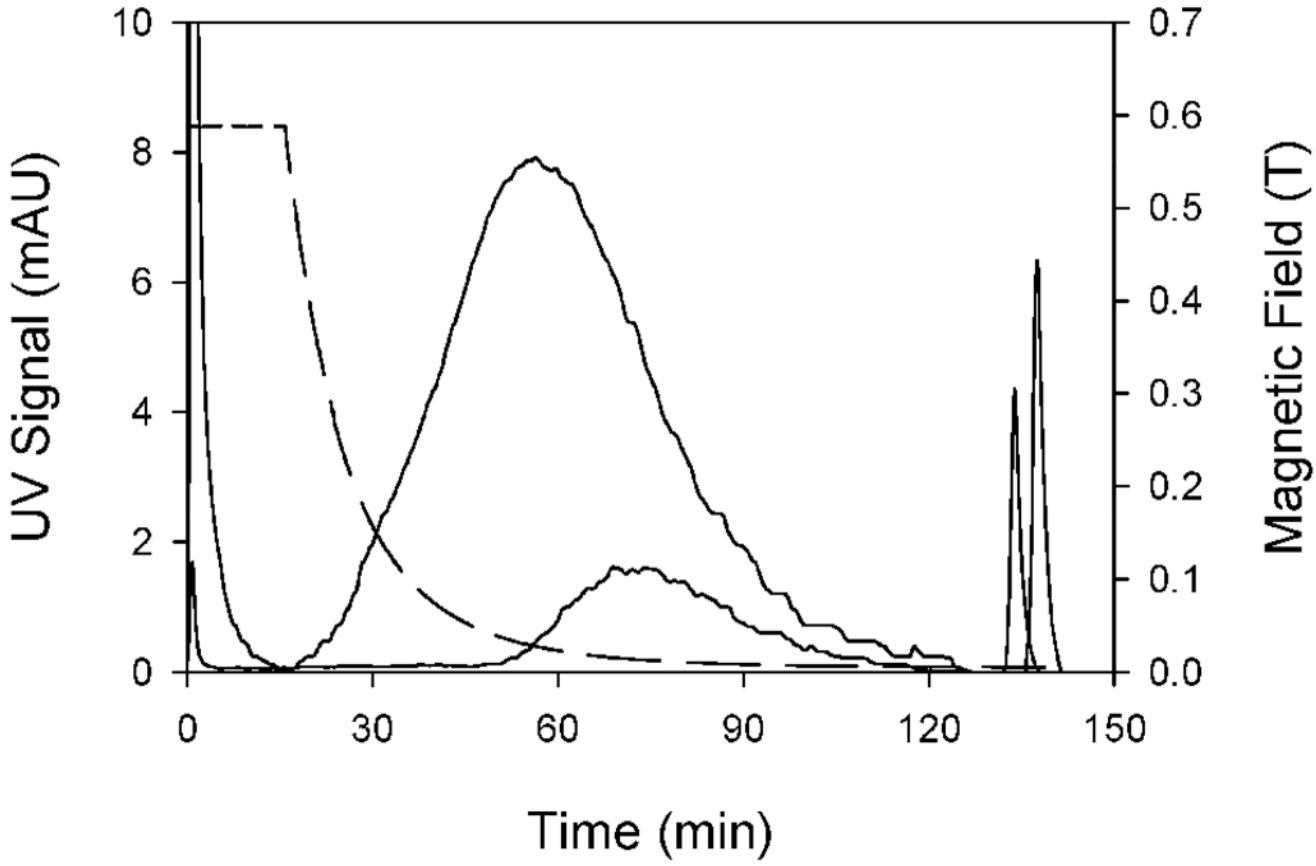

Figure 3.
Elution curves for the supplied magnetic nanoparticle sample (peak maximum at around 60 minutes), and for the fraction retained in the channel at 82 mT (peak maximum at around 75 minutes). The dashed line shows the decay of magnetic field at the outer channel wall (see right hand axis).

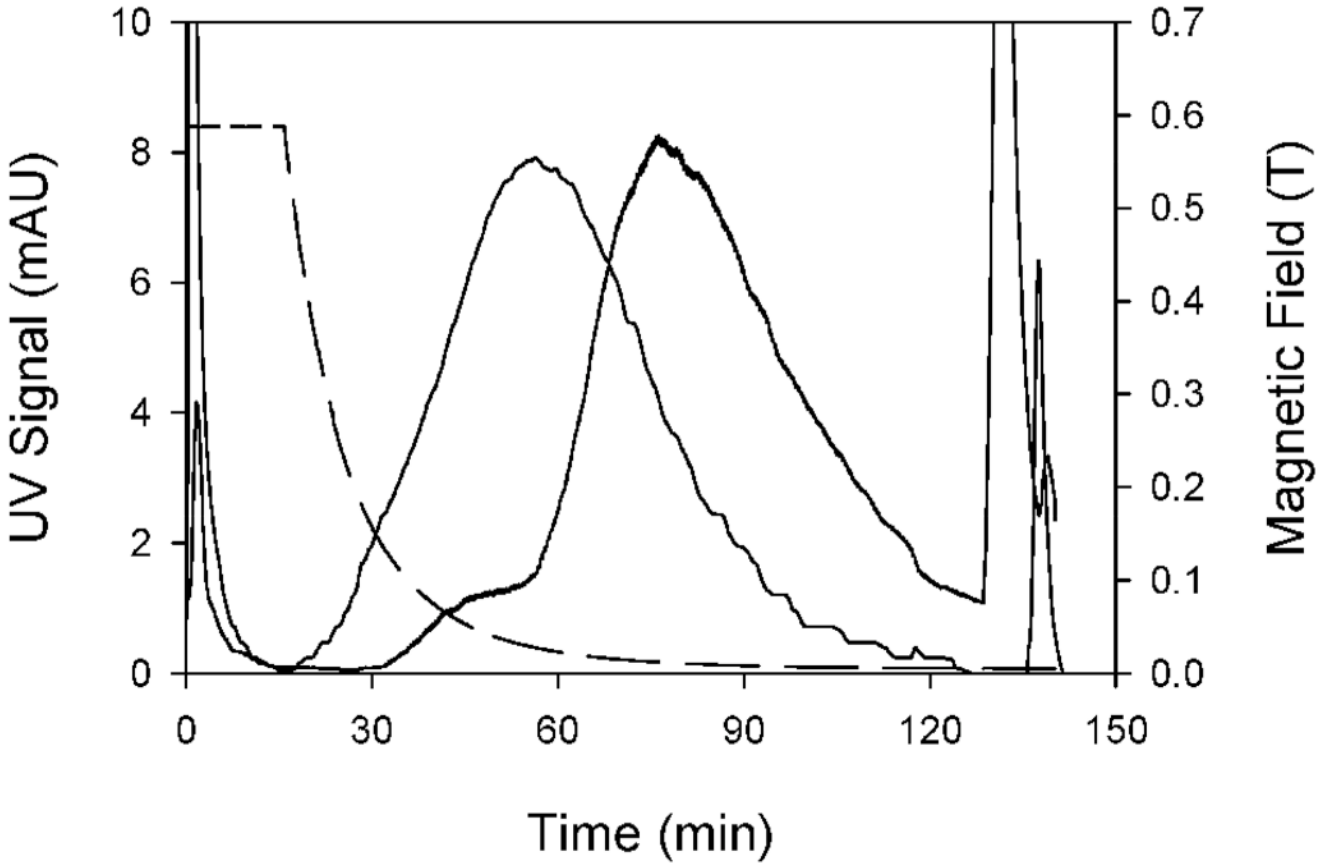

Figure 4.
Elution curves for the original magnetic nanoparticle sample (peak maximum at around 60 minutes), and for the fraction retained in the channel at 43 mT (peak maximum at around 80 minutes). The dashed line shows the decay of magnetic field at the outer channel wall (see right hand axis).

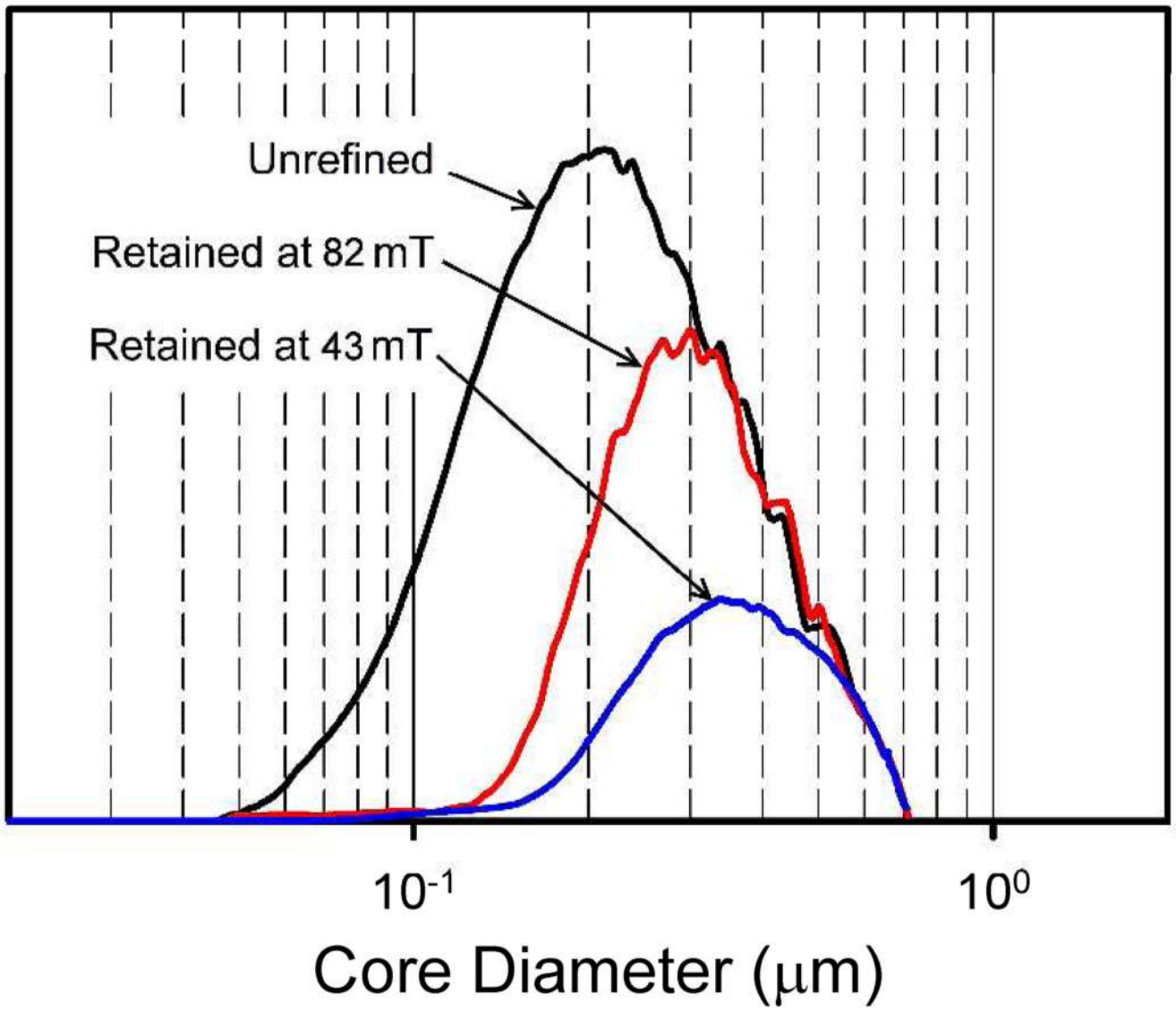

Figure 5.
The calculated equivalent spherical core diameter distributions on a logarithmic scale for the original magnetic nanoparticle sample, and for the samples collected after retention in the channel at 82 mT amd 43 mT.

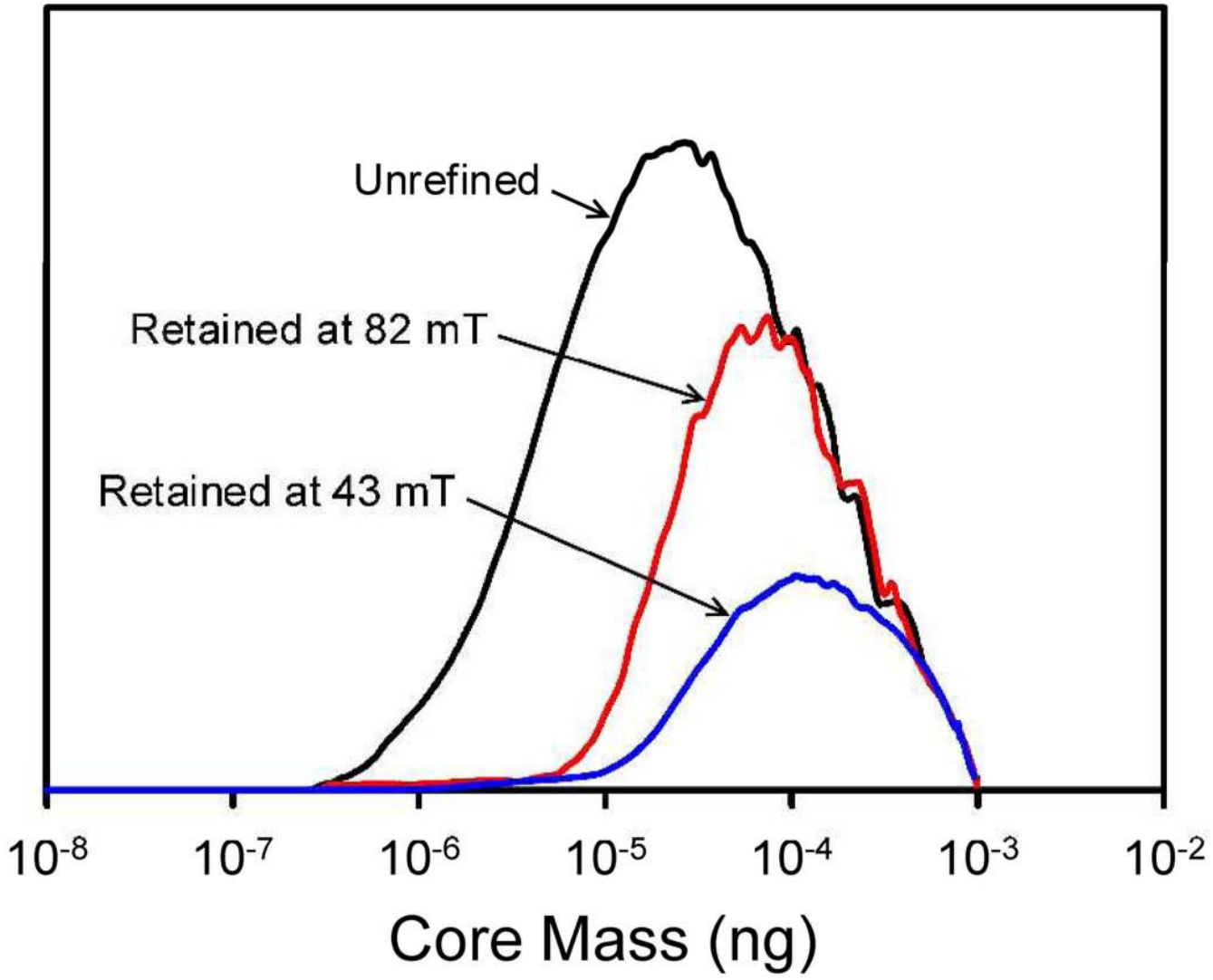

Figure 6.
The calculated magnetite core mass distributions on a logarithmic scale for the original magnetic nanoparticle sample, and for the samples collected after retention in the channel at 82 mT and 43 mT.